Chapter entitled: "Degradation of Spacecraft Materials"

Authors:
Joyce Dever, Bruce Banks, Kim de Groh and Sharon Miller
NASA Glenn Research Center

For inclusion in the
Handbook of Environmental Degradation of Materials

1. Introduction

Materials used on exterior spacecraft surfaces are subjected to many environmental threats which can cause degradation. These threats include photon radiation, charged particle radiation, temperature effects and thermal cycling, impacts from micrometeoroids and debris, contamination, and low Earth orbit atomic oxygen. Space environmental threats to materials vary greatly based on both the material and its environment. Environmental variables include orbital parameters for the mission, mission duration, the solar cycle and solar events, view angle of spacecraft surfaces to the sun, and orientation of spacecraft surfaces with respect to the spacecraft velocity vector in low Earth orbit. It is evident that each mission has its own unique set of environmental exposure conditions that must be well-understood for purposes of selecting durable spacecraft materials and interpreting observed degradation.

Fundamentally important properties for exterior spacecraft surfaces are structural integrity, and thermo-optical properties. Problems occur when spacecraft materials become too thin or brittle to support a required load or when protective thermal insulation film layers crack and peel away from the spacecraft. Operating temperatures of spacecraft systems rely on exterior surfaces possessing the required solar absorptance and thermal emittance values. Solar absorptance, α, is the fraction of incident solar energy that is absorbed by a surface. Thermal emittance, ε, is the ratio of radiated energy emitted from a

surface to that which would be emitted from a perfect (black body) emitting surface. Degradation of these thermo-optical properties can cause an undesirable change in temperature of the spacecraft or its components. Loss of transmittance through solar cell coverglass materials, such as through contamination, can result in decreased output of solar arrays, and, therefore, a reduction in overall spacecraft power. For electrical wiring and cables exterior to the spacecraft, resistivity of polymer insulation can be decreased upon space radiation exposure.

Understanding the degradation of spacecraft materials can be determined through space-exposures and ground laboratory studies. Each has advantages and disadvantages. Opportunities for examining space flown materials, through retrieved flight hardware or dedicated experiments, are rare. Dedicated space flight experiments are expensive and require long lead times from planning to flight. Differences between the experiment environment and the intended mission environment and synergistic environmental effects require cautious interpretation of results. Where it is not possible to retrieve spacecraft hardware, data available from satellite operations, such as power output and spacecraft surface temperatures, can also be used to assess material performance to some extent, but where severe degradation is evident, it is often not possible to conclusively identify the cause or mechanism of degradation, since comprehensive analysis of materials is not possible. Ground laboratory studies can be used to examine individual environmental effects or a combination of environmental effects. Laboratory tests can be conducted in a timely manner using accelerated levels for some environmental effects, but, due to the difficulties in exactly simulating the space effects, complex calibrations and cautious interpretation of the results are required. A combination of space exposures, ground laboratory studies and computational modeling is most useful for assuring durability of spacecraft materials.

This chapter includes descriptions of specific space environmental threats to exterior spacecraft materials. The scope will be confined to effects on exterior spacecraft surfaces, and will not, therefore, address environmental effects on interior spacecraft systems, such as electronics. Space exposure studies and laboratory simulations of individual and combined space environmental threats will be summarized. A significant emphasis is placed on effects of Earth orbit environments, because the majority of space missions have been flown in Earth orbits which have provided a significant amount of data on materials effects. Issues associated with interpreting materials degradation results will be discussed, and deficiencies of ground testing will be identified. Recommendations are provided on reducing or preventing space environmental degradation through appropriate materials selection.

2. Atomic Oxygen Effects

2.1. Environment Description

Atomic oxygen (AO) is formed in the low Earth orbital environment (LEO) by photo dissociation of diatomic oxygen. Short wavelength (< 243 nm) solar radiation has sufficient energy to break the 5.12 eV O_2 diatomic bond (Ref. 1) in an environment where the mean free path is sufficiently long (~ 10^8 meters) that the probability of reassociation or the formation of ozone (O_3) is small. As a consequence, between the altitudes of 180 and 650 km, atomic oxygen is the most abundant species (Figure 1) (Ref. 2). Although excited states of atomic oxygen can be formed, their lifetimes are sufficiently short that the ^3P ground state dominates the LEO atomic oxygen formation and is dependent upon the diatomic oxygen density and solar UV flux. Solar heating of the Earth's atmosphere causes an increase in the number density of atoms at a given altitude as the Earth rotates from sunrise toward solar noon. Because the atmosphere co-rotates with the Earth, the solar heated bulge in the atmosphere is pushed forward such that the peak of the atomic oxygen density occurs at approximately 3 P.M. rather than

solar noon. As a consequence, anti-solar facing surfaces such as the back side of solar arrays receive 25 percent more atomic oxygen fluence than the solar facing surfaces as the spacecraft orbits the Earth. (Ref. 3).

Solar-caused variations in the ultraviolet radiation impinging upon the LEO atmosphere can greatly change the atomic oxygen production rate (and therefore the arriving flux on spacecraft surfaces). Periods of high and low solar activity can change the arriving flux by a factor of up to 500 depending on altitude (Figure 2) (Ref. 2). Thus the atomic oxygen flux cannot be accurately predicted due to uncertainty in the solar activity. The average atomic oxygen fluence per year varies as a result of the solar activity consistent with the 11 years sun spot cycle as shown in Figure 3 based on the MSIS-86 atmospheric model (Ref. 4). Atomic oxygen can also be produced in other planetary environments where oxygen is present

As a spacecraft orbits the Earth at velocities on the order of 7.7 km/sec, it runs into the atomic oxygen (hence the term "ram" atomic oxygen). If the spacecraft is in an orbit that has zero inclination then the average angle of attack of the atomic oxygen is perpendicular to surfaces whose surface normal points in the direction of travel. However, most spacecraft have orbits which are inclined with respect to the Earth's equatorial plane. This causes the average angle of attack of the arriving atomic oxygen to sinusoidally vary around the orbit as a result of the vectoral addition of the orbital spacecraft velocity vector and the atmosphere's co-rotation velocity vector (Ref. 5). In addition, atomic oxygen atoms have thermal velocities associated with their Maxwell-Boltzman velocity distribution at the high temperatures of LEO which are typically ~1000 K (Ref 2). The high velocity tail of the Maxwell-Boltzman distribution actually allows some atomic oxygen atoms to catch up with the trailing surfaces

of a LEO spacecraft to produce a small flux which is orders of magnitude lower than the ram flux. Thus, the thermal velocities of the atomic oxygen associated with their Maxwell-Boltzman velocity distribution contributes as an additional component to the over all impact velocity of the atomic oxygen. If one adds the three vectoral components and averages over a typical 400 km orbit at 28.5° inclination, then angular distribution of arriving atoms is as shown in Figure 4, where the arrival distribution in the horizontal plane is shown as a function of incidence angle for surfaces normal to the ram direction. (Ref. 6).

Atomic oxygen can arrive at angles beyond 90° from the orbital direction. For example, Figure 5 shows that a surface whose normal is 90° with respect to the ram direction receives approximately 4% of the flux that occurs for a surface whose normal is parallel to the ram direction.

The impact energy of arriving atomic oxygen atoms also is dependent upon the following three contributions to the resulting velocity vectors: the orbital spacecraft velocity, the Earth's atmosphere co-rotation velocity, and atomic oxygen thermal velocity. Figure 6 is a plot of the energy distribution of atomic oxygen atoms as a function of altitude for a circular orbit with 28.5° inclination and 1000 K thermosphere. (Ref. 7). As can be seen, the average impact energy is 4.5 eV ± 1 eV for a 400 km orbit and the impact energy decreases with altitude. For highly elliptical orbits, the perigee ram impact energy can be significantly higher than for circular LEO orbits. Such elliptical orbits can also produce high fluxes near perigee due to the low altitudes involved. If a spacecraft is spinning with its axis of rotation perpendicular to the Earth then the average flux to any surface is simply $1/\pi$ of that of the ram direction.

2.2. Interaction with Materials

Although LEO atomic oxygen possesses sufficient energy to break most organic polymer bonds and sufficient flux to cause oxidative erosion of polymers, there was little known or interest in atomic oxygen interaction with materials until the start of space shuttle missions. This is primarily because most prior missions occupied high altitude orbits where atomic oxygen densities are rather inconsequential.

One evidence of LEO environmental interaction with materials is the glow phenomena that occurs when atomic oxygen and other LEO atmospheric species impact spacecraft surfaces causing the creation of short-lived excited state species that emit visible radiation near the surfaces of spacecraft as shown in Figure 7, where Figure 7a was taken during the daylight and Figure 7b was taken as a time exposure at night. (Refs. 8-10).

The reaction of atomic oxygen with spacecraft materials has been a significant problem to LEO spacecraft designers. Atomic oxygen can react with polymers, carbon and many metals to form oxygen bonds with atoms on the surface being exposed. For most polymers hydrogen abstraction, oxygen addition or oxygen insertion can occur (Figure 8). With continued atomic oxygen exposure, all oxygen interaction pathways eventually lead to volatile oxidation products accompanied by the gradual erosion of hydrocarbon materials. Surfaces of polymers exposed to atomic oxygen also develop an increase in oxygen content as shown in Figure 9 (Ref. 11).

The sensitivity of hydrocarbon materials to reaction with atomic oxygen is quantified by the atomic oxygen erosion yield of the material. The atomic oxygen erosion yield is the volume of a material that is

removed (through oxidation) per incident oxygen atom. The most well-characterized atomic oxygen erosion yield is that of polyimide Kapton® H which has an erosion yield of 3.0 x10^{-24} cm^3/atom for LEO 4.5 eV atomic oxygen (Refs. 12 and 13). Table 1 (Refs. 14-16) lists the atomic oxygen erosion yields of a wide variety of polymers, where many of the values are measured from space experiments and others are predicted values. The predicted erosion yield values (γ' mod-Correlation and 1/OI Correlation (Ref. 16)) listed in Table 1 were made based on predictive models, developed for the interaction of polymers with the LEO environment, and using information about the chemical composition, structure, and densities, as well as experimental data for Oxygen Index (Ref. 17).

The most common technique for determining the erosion yield of flight samples is through mass loss measurements. These measurements are made by obtaining mass measurements of the sample before and after flight. The erosion yield of the sample, E_S, is calculated through the following equation:

$$E_S = \frac{\Delta M_S}{(A_S \rho_S F)} \qquad (1)$$

where

E_S = *erosion yield of flight sample* (cm^3/*atom*)

ΔM_s = *mass loss of the flight sample* (*g*)

A_s = *surface area of the flight sample exposed to atomic oxygen attack* (cm^2)

ρ_s = *density of sample* (g/cm^3)

F = *fluence of atomic oxygen* ($atoms/cm^2$)

The atomic oxygen fluence, F, can be determined through the mass loss of a Kapton® witness sample because Kapton® has a well characterized erosion yield in the LEO environment. Therefore, the atomic oxygen fluence can be calculated using the following equation:

$$F = \frac{\Delta M_K}{(A_K \rho_K E_K)} \qquad (2)$$

where

ΔM_K = *mass loss of Kapton® witness sample (g)*

A_K = *surface area of Kapton® witness sample exposed to atomic oxygen* (cm^2)

ρ_K = *density of Kapton® witness sample (1.42* g/cm^3)

E_K = *erosion yield of Kapton® witness sample* (3.0×10^{-24} cm^3/*atom*)

Thus

$$E_S = E_K \frac{\Delta M_S A_K \rho_K}{\Delta M_K A_S \rho_S} \qquad (3)$$

One of the critical issues with obtaining accurate erosion yield data from mass loss measurements is making sure that dehydrated mass measurements are taken. Many polymer materials, such as Kapton, are very hygroscopic (absorbing up to 2% of their weight in moisture) and can fluctuate in mass significantly with humidity and temperature. Therefore, for accurate mass loss measurements to be obtained, it is necessary that the samples be fully dehydrated (e.g. in a vacuum desiccator) prior to measuring the mass both pre-flight and post-flight.

There is a large variation in the erosion yield values for the space data provided in Table 1. This is because some flight experiments were exposed to low atomic oxygen fluences on-orbit, such as during a shuttle flight experiment. Variations in much of the early LEO space data also as occurred because some erosion yield data were not determined based on dehydrated mass measurements, introducing large error for hygroscopic materials, especially for low fluence exposures or low erosion yield samples. The erosion yield values listed in Table 1 from References 15 and 16 represent more recent erosion yield values.

A LEO environment experiment called the MISSE (Materials International Space Station Experiment) PEACE (Polymers Erosion And Contamination Experiment) Polymers contains 41 different polymers for long term atomic oxygen erosion determination (Ref. 18). The MISSE PEACE Polymers samples were placed on the outside the ISS Quest Airlock in August 2001 during shuttle mission STS-105. The experiment is scheduled to be retrieved during STS-114, more than three years after its installation on ISS. The erosion yield data (to be obtained using dehydrated pre- and post-mass measurements) from this long-term International Space Station (ISS) experiment will be directly compared with the predictions provided in Table 1.

Atomic oxygen can also oxidize the surfaces of metals to produce nonvolatile metal oxides. However, for most metals, the oxides tend to shield the underlying metal from oxidation. Silver is one exception, because silver oxide tends to spall from the underlying metal thus allowing continued oxidation. Such effects caused silver solar cell interconnects to fail in LEO (Ref. 13). Atomic oxygen interaction with silicones causes oxidation and removal of methyl groups and gradual conversion of the surface of silicones to silica (Refs. 19-21). This frequently results in shrinkage and crack formation in the exposed

silicones (Figures 10 and 11) as they are transformed from low modulus polymers into the higher modulus silica.

Surfaces of materials with volatile oxidation products (such as hydrocarbon polymers), that are oriented in a fixed position with respect to the ram direction gradually develop left-standing cones which point in the direction of arriving atomic oxygen. Thus the microscopic roughness of the surfaces increases with time. Because the erosion of one location is independent of any other location and atomic oxygen arrives randomly, the development of surface roughness obeys Poisson statistics. This causes the surface roughness to increase as the square root of the atomic oxygen fluence (Ref. 22). Figure 12 shows typical atomic oxygen textured surfaces of Kapton® H polyimide, fluorinated ethylene propylene and chlorotrifluoroethylene after fixed-orientation exposure to atomic oxygen in LEO (Refs. 23 and 24). In addition to polymer thickness loss, such texturing causes an increase in diffuse reflectance and a decrease in specular transmittance of polymers (Ref. 25). Atomic oxygen exposure of hydrocarbon or halocarbon polymers that are pigmented or filled with metal oxide particles results in erosion of the polymeric content resulting in gradual exposure of an increasing surface population of metal oxide particles which are poorly attached to each other (Ref. 26). The metal oxide particles, which become loosely attached, remain in contact and gradually shield the underlying polymer content from atomic oxygen erosion Thus the erosion yield can gradually decrease with atomic oxygen fluence.

2.3. Mitigation Techniques

Atomic oxygen erosion of thin polymers in LEO has represented a challenging spacecraft performance and durability problem for many years. Three approaches have been taken in efforts to reduce or eliminate atomic oxygen erosion of polymers. The three approaches to achieve polymer durability to

atomic oxygen consist of: 1) the application of thin film protective coatings made of atomic oxygen durable materials, 2) the modification of the surface of the polymers to make them more durable to atomic oxygen, and 3) the use of alternative polymers that contain metal atoms which develop a protective coating with atomic oxygen exposure.

The first and most widely used mitigation approach is the application of thin film metal, metal oxide or fluoropolymer-filled metal oxide protective coatings to polymers (Refs. 27-31). Thin film coatings of SiO_2, Al_2O_3, Indium Tin Oxide, Ge, Si, Al, and Au with thickness ranging from a few hundred to more than 100 nm are typically applied by sputter deposition or vapor deposition. For example, the SiO_2 coatings on Kapton® H polyimide for the solar array blankets on the International Space Station are 130 nm thick and applied by magnetron sputter deposition. (Ref. 32). Although metal oxide coatings as thin as ~5.0 nm can provide atomic oxygen protection on ultra smooth surfaces, usually thicknesses of ~100 nm are used to assure complete coverage over irregularities of debris, pits and rills on polymer surfaces. Coatings which are factors thicker than 100 nm can more easily crack or spall due to either their intrinsic stress or inability to conform with flexure compression or expansion at their polymer substrates. The addition of fluoropolymer content to metal-oxide coatings allows factors greater strain-to-failure in the coatings. Such coatings can be deposited by co-sputter deposition of SiO_2 and polytetrafluoroethylene Teflon® (Refs. 25 and 27).

The atomic oxygen durability of polymers, that are protected by thin film coatings made of materials which are themselves atomic oxygen durable, is largely dependent upon the number and size of pinwindow and scratch defects in the protective coatings. (Figure 13) The application of 130 nm SiO_2 protective coatings on Kapton® polymide can frequently reduce the rate of weight loss due to atomic

oxygen erosion of Kapton® to less than 1% of that of unprotected Kapton® (Ref. 32). Atomic oxygen undercutting oxidation at sites of pin window and scratch defects can ultimately lead to mechanical failure of the polymer when a sufficient number of undercut cavities connect (Ref. 29). The growth of undercut cavities has been studied for polymer films coated on one side or both sides through the use of Monte Carlo computational modeling (Refs. 7, 33-36).

One approach to reducing the number of pinwindow and scratch defects in atomic oxygen protective coatings is to apply a surface tension leveling coating to the material prior to applying the protective coating. Studies have found the use of leveling coatings successful for increasing the atomic oxygen durability of protective coatings on composite materials based on decreasing defect densities (Refs. 37 and 38). For example, in one study a low viscosity epoxy was applied to the surface of several composite coupons. A protective layer of 1000 Å of SiO_2 was deposited on top of the leveling coating, and the coupons were exposed to an atomic oxygen environment in a plasma asher. Pinhole populations per unit area were estimated by counting the number of undercut sites observed by scanning electron microscopy. Defect density values of 180,000 defects/cm^2 were reduced to about 1000 defects/cm^2 as a result of the applied leveling coating (Ref. 37) Leveling coatings have also been found to improve the optical performance of composite concentrator surfaces by improving the specular reflectance (Refs. 37 and 38).

The mitigation approach involving modification to the surface of polymers to make them more durable to atomic oxygen has primarily involved either implantation of metal atoms into the surface of the polymer (Ref. 39) or chemical modification of the surface of the polymer to incorporate silicon atoms into the surface and near surface. In both surface modification approaches the degree to which the

atomic oxygen erosion yield is reduced is dependent upon the aerial density of metal atoms that can be placed into the polymer surface.

The formation of alternative polymers that contain inorganic atoms has been approached through a variety of chemical formulations including the use of silicone co-polymers (Ref. 40), polysilsesquioxane (Ref. 41), cage coordination compound incorporation of metal atoms (Ref. 42) and phosphorous containing polymers (Ref. 43). As with the surface alteration approach, the durability of the alternative polymer is dependent upon the aerial density of inorganic atoms that can be achieved. In addition, the alternative polymers must achieve the durability to other space environmental threats such as UV radiation and ionizing radiation to be considered a suitable replacement for Kapton® polymide. However, some of the alternative polymers have the advantage of much lower solar absorbtance than Kapton® (Ref. 43).

3. Contamination Effects

3.1. Sources and Transport of Spacecraft Contamination

Spacecraft contamination can be defined as molecular or particulate matter on or near a spacecraft surface that is foreign to that surface. Sources of spacecraft contamination can include thruster propellants and burn residue, outgassing of spacecraft materials, vented gases from spacecraft systems, fluids released from the spacecraft by dumping or leakage, micrometeoroids and orbital debris, and particles generated or redistributed during spacecraft mechanical operations or astronaut extravehicular activity (EVA) operations (Ref. 44). Comprehensive data on outgassing of spacecraft materials is found in Ref. 45. Space environment interactions with materials can also produce contaminants, such as volatile products of atomic oxygen reactions and ultraviolet-induced or radiation-induced chain scission

products in polymer materials and residual non-oxidative films left free-standing due to AO erosion of underlying material. Space environment effects, such as atomic oxygen, ultraviolet, and radiation interactions, can further modify contaminant species.

Spacecraft contaminants can either deposit onto spacecraft surfaces or remain in the vicinity of the spacecraft. Molecular contaminants can transport from surface-to-surface through various mechanisms including line-of-sight transport, non-line-of-sight transport through reflection or scattering, and attraction of positively ionized contaminants to a negatively charged, sunlit spacecraft surface (Ref. 46). These transport mechanisms can put critical spacecraft surfaces at risk for contamination effects.

3.2. Contamination Effects on Spacecraft Surfaces

Buildup of molecular or particulate spacecraft contamination can cause degradation in transmittance, reflectance, solar absorptance, and thermal emittance of surfaces. The impacts of this degradation include reduced performance of solar arrays, radiators, instrument optics, sensors, and other systems (Ref. 44).

Some particularly detrimental cases of space environment interactions with spacecraft contamination include AO oxidation of outgassed silicones to produce a non-eroding silica-based layer, and ultraviolet or ionizing radiation interactions with contaminants to produce a contaminant film. Examples of these cases will be discussed below.

3.2.1. Atomic Oxygen Interaction with Silicones

Almost all spacecraft have silicones on board in the form of adhesives, potting compounds and lubricants used in materials processing. Although most LEO spacecraft designers make efforts to use only silicones that are vacuum stripped to eliminate or reduce the amount of volatile short chain content, silicone fragments are often evolved in the vacuum environment in LEO with the process being further enhanced with AO and/or radiation-induced bond breaking. The resulting silicone fragments can deposit on surfaces that are exposed to atomic oxygen. If the surfaces are not receiving atomic oxygen, then simple re-evaporation of the silicone can occur providing that the surfaces are the same temperature or hotter than the source of the silicone. Or, UV may interact with the silicone fragments causing a polymerized contaminant layer to build up, as will be discussed in Section 3.2.2. With atomic oxygen arrival, oxidation reactions cause the silicones to lose hydrocarbon content and convert to a silica-based surface layer which is resistant to atomic oxygen erosion. Such processes occurred on the MIR Space Station resulting in the accumulation (over a ten-year duration) of a microscopically rough coating on the solar array (Figure 14) which was up to 4.6 μm thick (Ref. 19). Such coatings tend to be rather transparent. However if the silicone deposition is also accompanied by hydrocarbon deposition, a much more optically absorbing coating can result (Ref. 47). Figure 15 is a photograph of the anti-solar side of the same MIR solar array. The contamination is much more absorbing. It appears as a tan colored silica deposit formed by atomic oxygen reaction of silicones that were arriving at the same time hydrocarbons could arrive from a polymer mesh behind the array. The contaminant layer was ~ 1.24 μm thick.

The Long Duration Exposure Facility (LDEF) satellite, which was exposed for 69 months in the LEO environment, provided an interesting study of contamination processes as the leading edge received a high fluence of directed ram AO along with solar exposure, and the trailing edge received very little AO along with similar solar exposure. The resulting molecular contamination process on LDEF was the

removal of hydrocarbon based contaminants, and oxidation of silicone fragments on the leading edge (silica-rich, hydrocarbon-poor contaminant films), and the build-up of hydrocarbon contaminants and silicone fragments which were UV darkened on the trailing edge (hydrocarbon-rich, silicone contaminant films).

3.2.2. Photochemical Deposition of Contaminants

In the presence of UV light, contaminants can form a polymerized film on a spacecraft surface (Ref. 46). It has also been stated that charged particles may play a role in this polymerization process, either separately or synergistically. (Ref. 44) Even though outgassing rates decrease with time, subsequent contaminant deposition rates do not decrease at the same rate. This is because photochemical contamination processes have been found to continue even when outgassing has subsided. (Ref. 44) This can be a significant concern to long-duration missions.

3.3. Mitigation of Contamination Effects

Mitigation of spacecraft contamination effects is achieved through careful selection of materials, particularly low outgassing materials, a spacecraft design which minimizes contamination risk for critical components, and taking precautions for spacecraft cleanliness during ground assembly and on-orbit operations. Spacecraft materials outgassing data is found in (Ref. 45), and detailed guidelines for spacecraft contamination control can be found in Ref. 48.

4. Space Radiation Effects

4.1. Solar Ultraviolet Radiation

4.1.1. Environment Description

Earth's atmosphere absorbs all ultraviolet radiation from the Sun that is less than 0.3 microns in wavelength (Ref. 46); however, spacecraft outside of the Earth's atmosphere and with a view of the Sun are subject to the full solar spectrum. Additionally, spacecraft surfaces without a direct view of the sun, but with a view of Earth, may still experience solar ultraviolet effects due to Earth albedo, which is the Sun's energy (~31%) reflected back to space by the Earth's atmosphere (Ref. 46). The solar spectrum outside the Earth's atmosphere at one astronomical unit from the Sun is referred to as the air mass zero solar (AM0) spectrum and is shown in Figure 16 (Ref. 49). In general, the ultraviolet range is defined as the portion of the electromagnetic spectrum including wavelengths between 4 nm and 400 nm (Ref. 50). However, relevant to materials degradation in space, it is convenient to examine only those wavelengths which are significant in the AM0 solar spectrum. Integrated solar irradiance in various wavelength ranges are shown in Table 2 (Ref. 49) along with the portion of the solar constant represented by each wavelength range. It is evident that wavelengths shorter than approximately 120 nm represent a negligible portion of the solar spectrum. Relevant to the study of space environment effects on materials, the ultraviolet range of wavelengths can be conveniently divided into two bands: Near UV (NUV) as the 200-400 nm range and vacuum UV (VUV) as the 100-200 nm range.

4.1.2. Effects on Materials

Polymers are particularly susceptible to ultraviolet radiation degradation, because many types of bonds in organic polymers are capable of absorbing UV light which can lead to photochemical reactions (Refs. 46 and 51). Additionally, impurities, which are usually contained in synthetic polymers, are often more likely to absorb UV light than the polymer itself, and can be significant contributors to the photochemical reactions within the polymer material (Ref. 51). Photochemical reactions within organic molecules may result in effects such as discoloration of the material (increase in solar absorptance) or

loss of mechanical properties due to chemical changes in the material. Important considerations for polymer UV durability in space are the wavelengths required to cause degradation, the depth of degradation, and synergistic effects with other environmental factors. It is generally thought that most polymers absorb approximately 95% of incident radiation below 250 nm within 0.3 μm from the surface (Ref. 52). However, based on the data shown in Figure 17, Teflon® FEP is an exception as it transmits a significant amount of ultraviolet radiation through tens of micrometers in depth (Ref. 53).

For polymer films whose thickness is significantly greater than the UV attenuation depth, the depth within which the majority of UV light as absorbed, the undegraded portion of the polymer thickness provides support to a degraded surface. However, for applications using polymer films whose thickness is on the order of the UV attenuation depth, the potential for UV degradation resulting in cracking of the full film thickness is significant.

Glass and ceramic materials have been observed to undergo ultraviolet radiation-induced darkening (Refs. 50 and 54), also referred to as "solarization". UV light interactions in glass and ceramic materials can cause formation of electrons or holes which are trapped in various defects. Some of these trapped species absorb light in specific wavelength ranges and are referred to as color centers. (Ref. 54) Many factors have been found to affect UV-darkening, including purity of the material, particle shape and size, surface chemistry and thermal history (Ref. 55). UV darkening is detrimental to spacecraft materials such as white paint coatings and solar cell cover glass.

In order to understand effects of space ultraviolet radiation on materials, it is useful to examine results of laboratory testing reported in the literature. However, results should be cautiously interpreted, because

there are a multitude of variables associated with ultraviolet testing which make it difficult to compare results directly from one test to another. These variables include: wavelength range, spectral shape and intensity of the UV source, and the nature of the exposure environment (air, purge gas, or vacuum). It is important to note that UV-induced degradation reactions in polymers are also influenced by oxygen, where the quantum yield (i.e. number of scission products per incident photon) is often greater for reactions in the presence of oxygen (Refs. 51 and 56), and, even vacuum systems contain some amount of oxygen from residual air in the system. For some materials, especially semiconductor pigmented paints, post-irradiation exposure to air, as is often required for post-exposure analysis, can cause reversal of the UV-induced damage, sometimes referred to as "air bleaching," creating an additional complication for interpreting test results (Ref. 55).

4.1.2.1. Effects on Fluoropolymers

UV interactions with fluoropolymers have been found to cause loss of mechanical properties and loss of optical properties. Erosion, mass loss, and surface roughness increases have been observed for Teflon® fluorinated ethylene propylene (FEP) upon exposure to a broad spectrum (> 115 nm) VUV deuterium lamp providing wavelengths greater than 115 nm in vacuum (Refs. 57 and 58), and erosion of FEP was also observed upon exposure to monochromatic light of 147 nm (Ref. 58). Broad spectrum VUV (> 115 nm) also caused mechanical properties degradation for FEP (Ref. 58). One study (Ref. 59) examined effects of broad spectrum VUV light on FEP using windows to produce lower cut-off wavelengths of 115 nm, 140 nm, and 155 nm. All wavelength ranges were found to produce degradation in the strength and elongation-to-failure of FEP, indicating that wavelengths greater than 155 nm are capable of degrading FEP. In another study, surface hardness of FEP was found to increase as a function of increasing exposure to broad spectrum VUV (> 115 nm), where surface hardness was used as a measure

of surface embrittlement. In this test, surface hardness was analyzed using atomic force microscopy (AFM) techniques (Ref. 60). Teflon® polytetrafluoroethylene (PTFE) was found to be more susceptible to UV damage than FEP (Ref 58).

Various synergistic effects were observed for fluoropolymers exposed to ultraviolet radiation during heating or thermal cycling. Tensile strength and elongation-to-failure were found to decrease for PTFE polymers upon UV exposure in the 185-369 nm wavelength range in vacuum or nitrogen at temperatures of 21 °C to 315 °C suggesting that chain scission occurs in PTFE polymers (Ref. 61). UV exposure of FEP resulted in chain scission at ambient or slightly higher temperatures, and cross-linking above 80 °C (Ref. 61). VUV exposure (147 nm light) at temperatures of 120 °C and 150 °C resulted in a significant decrease in tensile strength and elongation compared to the negligible change observed for VUV alone (Ref. 58). Compared to VUV irradiation with steady-state heating at 100 °C, creep deformation increased for VUV irradiation with thermal cycling, which was attributed to FEP traversing between phases during thermal cycling (Ref. 62).

Tedlar® (polyvinyl fluoride) is found to undergo loss of strength and elongation due to ultraviolet exposure as reported in the literature for terrestrial uses of Tedlar® (Ref. 63). Regarding testing for aerospace applications, Tedlar® materials were exposed to at least 2500 equivalent sun hours in a facility that provided vacuum UV (> 115 nm) and near UV (~200-400 nm) to simulate LEO and GEO solar conditions (Ref. 64). Results from this test showed that solar absorptance for an uncoated cloud white Tedlar® increased. Use of an Optical Coating Laboratory, Inc. (OCLI) multi-layer coating prevented a significant change in solar absorptance. The OCLI coating was thus found to perform well as a UV

protective coating for white Tedlar®. However, another investigation showed that an OCLI coating did not adhere well to FEP (Ref. 60), which will be described in section 5.2.3.

Whereas VUV radiation from a deuterium lamp ($\lambda > 115$ nm) was found to cause mass loss of FEP, no mass loss was observed for unpigmented Tedlar® (Ref. 65). Lack of mass loss for Tedlar® was attributed to the fact that, unlike FEP, Tedlar® contains CH bonds. It was proposed that Tedlar® undergoes cross-linking which modifies the surface layer.

As illustrated through the examples above, ultraviolet radiation and synergistic effects with heating or thermal cycling are well-known to cause degradation of mechanical properties and optical properties of fluoropolymers. The degree to which degradation occurs depends upon irradiation wavelengths, exposure temperatures, and the chemical nature of the fluoropolymer.

It is important to note that the spectral mismatch between the VUV deuterium lamp and the AM0 Sun may produce degradation mechanisms that are different between space and laboratory exposures. For example, the lamp's peak at around 160 nm coincides with a peak of Teflon® UV absorption (Ref. 66). There is no such peak in the solar spectrum. The VUV lamp peak may result in enhanced surface reactions for Teflon® which would not occur to as great an extent in space.

4.1.2.2. Effects on Polyimide Kapton

Polyimide Kapton® shows minor changes in properties upon VUV exposure. In one study (Ref. 67), a sample of 25.4 μm Kapton® HN exposed to 1100 equivalent VUV sun hours (115-200 nm range) did not experience any statistically significant changes in elongation or ultimate tensile strength. Minor changes in the reflectance spectrum in the ultraviolet-visible wavelengths due to this exposure may be indicative

of some changes in surface chemistry, however. A minor increase in solar absorptance due to this VUV exposure, from approximately 0.23 to approximately 0.24, was also observed.

4.1.2.3. Effects on Epoxy Composites and Adhesives

In one study, it was found that UV exposure (220-300 nm wavelength range) of epoxy resin caused degradation within the top 0.5 to 1.0 μm layer) for exposure as little as 30 minutes of exposure (Ref. 68). Weight loss of epoxy composite materials was observed and was found to increase with increased UV irradiation time for a test conducted using an accelerated weathering tester consisting of medium-wave UV (200-300 nm) lamps in a system controlled at 50 °C (Ref. 69). Another test found that UV irradiation from medium-wave (200-300 nm) UV lamps initiated microcracks in graphite epoxy and glass epoxy composites, which then propagated upon thermal shock testing between 121 °C and liquid nitrogen temperature (-196 °C) (Ref. 69). On the Long Duration Exposure Facility (LDEF), which exposed materials to the space environment for 69 months, Hysol 934 epoxy adhesive was found to discolor and Hysol EA 9628 was found to have a decreased shear strength following flight. These effects were attributed to UV degradation (Ref. 70).

4.1.2.4.Effects on White Paint Coatings

Space-stable coatings with low solar absorptance and high thermal emittance are important to spacecraft thermal control. Z93 and YB-71 paints, with zinc oxide and zinc orthotitanate pigments, respectively, in potassium silicate binders, have proven to maintain their thermo-optical properties in the space environment (Ref. 55). A paint formulation with zinc oxide pigment in a methyl silicone binder, designated as S13G/LO, provides a more flexible option for the white paint coating. (Ref. 55). Development of these three types of paints originated based on the UV stability of the ZnO and Zn_2TiO_4

pigments. Other pigments examined were found to undergo significant UV degradation, including, zirconia, alumina, and silica pigments (Ref. 55). Although Z93, YB-71 and S13G/LO paints have shown appropriate space stability, the S13G/LO material degrades in UV somewhat faster than YB-71 or Z93, and, therefore, its use is limited to shorter duration missions. For example, for 5000 equivalent sun hours of UV exposure, solar absorptance increases of ≈0.02, 0.03, and 0.06 are were observed for YB-71, Z93, and S13G/LO, respectively (Ref. 55).

4.2. Ionizing Radiation

The ionizing radiation environment of space includes energetic charged species such as electrons and protons and energetic photons such as x-rays and gamma rays. These energetic particles and photons are considered ionizing radiation because they ionize atoms as they move through a material. The extent of high energy particle interactions with materials depends upon the type of radiation, its energy and the material. Details on the interactions of radiation with matter are comprehensively addressed elsewhere (Refs. 71 and 72). Many materials degrade due to the total ionizing dose, or the amount of energy deposited into a material, although, for some properties, dose rate affects the damage. Radiation dose, referred to in SI units of grays (Gy), is the amount of radiation that deposits 1 J of energy per 1 kg mass of material. Another commonly used unit is the rad, which is 0.01 Gy. Sources of ionizing radiation within the space environment are described below.

4.2.1. Solar Flare X-ray Radiation Environment

Solar flares are releases of intense energy from the Sun occurring over a short duration (minutes to hours) observed as sudden brightening of the chromosphere of the Sun and producing energy throughout the electromagnetic spectrum from radio waves to gamma rays (Refs. 46 and 73). During the

approximately 11-year solar cycle, periods of high solar activity are correlated with enhanced X-ray emission (Ref. 46).

For spacecraft in Earth orbits, surfaces with a view of the sun during periods of solar flares will be exposed to a significant flux of X-rays. The Geosynchronous Operational Environmental Satellites (GOES) have been monitoring the space solar X-ray environment since 1986, from their location in geosynchronous orbit at an altitude of approximately 35,800 km. GOES solar X-ray flux data, available through the National Oceanic and Atmospheric Administration (NOAA) National Geophysical Data Center (NGDC) (Ref. 74) were used to estimate the solar flare X-ray environment in wavelength regions of 0.1-0.8 nm, 0.05-0.4 nm, and 0.0124-0.05 nm for the Hubble Space Telescope mission in LEO (Ref. 75). These X-ray fluences and estimated dose depth profiles for FEP are shown in Figure 18.

4.2.2. Charged Particle Radiation Environment

The three main sources of charged particle radiation naturally occurring in space are galactic cosmic rays, solar proton events, and the trapped radiation belts. Galactic cosmic rays (GCRs) consist of low flux ionized nuclei, mostly protons, generally providing a very low radiation dose rate, which is highest at solar minimum. (Ref. 46). GCR radiation consists of ions of all elements of the periodic table and is composed of approximately 83% protons, 13% alpha particles (^{4}He ions), 3% electrons, and 1% of heavier nuclei (Ref. 76). Energies of GCR particles range from about 10^8 to 10^{19} eV (Ref. 46). Low altitude/inclination orbits are protected from some of the GCRs, because when a GCR approaches Earth in the plane of the equator, Earth's magnetic field bends the particle back to space or to the polar regions, depending on its initial direction and energy (Ref. 46). Solar proton events (SPEs) result from coronal mass ejections producing significant proton flux over short duration periods of, on average, one to five days (Ref. 46). Some SPE's are heavy ion rich with energies ranging from 10's of MeV/n to

100's of GeV/n (Ref. 76). Spacecraft in low Earth orbits, such as the Hubble Space Telescope, are generally protected by the magnetosphere from the majority of SPE proton flux, but SPE's are hazardous to spacecraft in high inclination orbits and geosynchronous orbit (Ref. 75). In the trapped radiation belts, also called the Van Allen belts, energetic electrons and protons are confined to gyrate around Earth's magnetic field lines. Trapped electrons have energies up to 10's of MeV and trapped protons and heavier ions have energies up to 100's of MeV (Ref. 76). Fluxes of protons and electrons in the trapped radiation belts are a function of particle energy, altitude, inclination, and solar activity and can increase during solar storms (Refs. 46 and 76). Peak fluxes of both electrons and protons occur at around 3000 km and a second peak of electron flux occurs at around 25,000 km altitude (Ref. 46). Additional variables affecting trapped radiation flux include effects of Earth's poles and the South Atlantic Anomaly. Spacecraft in polar orbits experience greater charged particle dose rates than spacecraft in equatorial orbits due to Earth's magnetic field funneling charged particles into the polar regions (Ref. 46). An asymmetry in Earth's magnetic field lines causes charged particles to reach lower altitudes (< 1000 km) in the South Atlantic, so that spacecraft experience higher dose rates during passage over this region (Refs. 46 and 76).

Estimates of the trapped proton and electron fluences have been obtained using NASA's proton (AP-8) and electron (AE-8) models (Refs. 77 and 78). The trapped electrons and protons are considered to be omni-directional by the AP-8 and AE-8 models, although some degree of east-west asymmetry has been observed by spacecraft measurements in the time since these models were developed (Ref. 77). Because of the approximately omni-directional nature of the trapped radiation, all exterior spacecraft surfaces are exposed to this radiation.

4.2.3. Space Ionizing Radiation Effects on Materials

4.2.3.1. Polymers

Ionizing radiation interacts with atomic nuclei and their surrounding electron clouds without specificity to particular chemical bonds, unlike ultraviolet radiation which is absorbed by particular chemical bonds (Ref. 79). Polymers can become degraded in physical and mechanical properties due to accumulated total dose of ionizing radiation, which includes electrons, protons and X-rays and GCRs.

Polymer films, such as FEP and Kapton, are commonly used on exterior spacecraft surfaces for thermal control blankets and adhesively bonded radiator surfaces, and, therefore, receive an unshielded dose of space radiation. Embrittlement and loss of strength are not significant concerns for radiator surfaces rigidly adhered to metal structures; however, for polymer films that are not rigidly supported such as in multilayer insulation applications, degradation in mechanical properties can result in cracking of the exterior polymer film layers. Cracking in thermal blanket layers can compromise the thermal protection of underlying equipment and may pose a contamination risk if pieces of the cracked film become dislodged. In addition to thermal insulation blankets, other uses of polymers on spacecraft exterior surfaces include structural composites, adhesives, potting materials, and wiring/cable insulation.

As a guide to effects of radiation on spacecraft polymers, Table 3 shows the ionizing radiation doses that have been found to produce mild to moderate and moderate to severe polymer degradation (Ref. 80).

Relative degradation data such as in Table 3, which are found commonly in radiation effects references and which vary slightly among references (see also Ref. 46 and Ref. 81) can be used as a screening tool for materials selection, but it is important to consider that many other factors may play a role in overall materials degradation in a space radiation environment. For example, the uniquely low solar

absorptance and high thermal emittance of FEP have led to its wide use for spacecraft thermal control, despite its susceptibility to radiation degradation.

Whereas the data in Table 3 are for polymers exposed to gamma radiation in air, it is generally found that irradiation in oxygen or air produces more severe degradation of polymers than irradiation in vacuum. For example, air or oxygen is known to significantly affect the radiation-induced degradation of PTFE, which undergoes scission at a much higher yield in air than in vacuum (Ref. 79). A similar finding was reported for x-ray irradiated Teflon® FEP which experienced an increase in the degradation of mechanical properties after air exposure (Ref. 82). Also, many polymers which predominantly crosslink when irradiated in vacuum will undergo main chain scission when irradiated in air, indicating that not just the extent of degradation is affected by the exposure environment, but the mechanism of degradation as well (Ref. 79).

Table 3 does not account for dose rate effects or synergistic effects of radiation and temperature. One report summarized that long-duration low dose rate exposures produced greater degradation of FEP than short duration high dose rate exposure, indicative of a possible dose rate effect, however, this apparent dose rate effect was attributed to time spent at elevated temperatures rather than to dose rate alone. (Ref. 61). This report stated that accelerated ground testing for ionizing radiation degradation to FEP may underpredict in-space damage by factors of 3-10, as a crude guideline. Further synergistic considerations for radiation and temperature are discussed in section 5.2.3.

Newer applications for polymer films on spacecraft require large, lightweight, deployable and/or inflatable spacecraft structures, requiring significantly thinner materials than used in thermal blanket

applications. Decreasing the thickness of a polymer increases the risk for radiation damage effects. This is because space ionizing radiation deposits a decreasing dose at increasing depths within a material, so that the greatest damage to a polymer film is at the surface and the damage decreases with increasing depth. An example of dose vs. depth in FEP, a widely used and radiation-vulnerable material, is shown in Figure 18 for solar flare x-rays and trapped electron and proton radiation.

When ionizing radiation degradation is combined with ultraviolet degradation, another effect that diminishes with increased polymer thickness, it is evident that ultra-thin polymer films, such as gossamer structures, are at great risk of radiation-induced degradation. Because of the greater radiation sensitivity for thinner polymer films, accurate modeling of the space environment and associated dose-depth profiles for polymer films is critically important to predicting the durability of thin polymer films for use on large spacecraft structures for long-duration missions. Methods of modeling the space environment are described in (Refs. 80 and 81) and methods for developing appropriate dose-depth profiles and space radiation simulation tests are described in Ref. 81.

Some newer polymer film materials have been studied for radiation durability applicable to use in deployable and inflatable spacecraft structures. Two studies (Refs. 83 and 84) examined effects of electron and proton radiation, in some cases with ultraviolet radiation as well, on aromatic polyimide films to simulate exposure near the Earth-sun Lagrangian points 1 and 2. Films tested included Kapton® HN, Kapton® E, Upilex® S, CP-1, CP-2 and either TOR-RC (Ref. 83) or TOR-LM (Ref. 84). All materials were found to undergo increased solar absorptance due to the radiation exposure.

In addition to polymer mechanical degradation, electrical properties of polymers may also be compromised due to radiation. This is a particularly important effect for polymers used for electrical insulation, such as wiring or cable insulation. Ionizing radiation has been found to induce conductivity in polymer films (Ref. 85). This induced conductivity has been found to be material-dependent and dose rate-dependent, but independent of the type of ionizing radiation (Ref. 85). One study examined radiation-induced conductivity in various polymers upon exposure to gamma rays to up to 10^6 Gy (Ref. 86). This study found increases in conductivity for polyethylene and polystyrene of 2-3 orders of magnitude, less than an order of magnitude increase for Teflon®, and negligible increases in conductivity for nylon, epoxy, and polyvinyl chloride. This induced conductivity has been found to be temporary, however. Once the radiation exposure was discontinued, those materials which experienced radiation-induced conductivity recovered to near-initial conductivity within seconds to hours (Ref. 86).

One complication of accelerated rate charged particle radiation testing of polymer materials is the possibility for charging of insulating polymer surfaces. PTFE, for example, is an excellent electrical insulator. On-orbit, the low current and dose rates permit continuous discharge of exposed PTFE materials. However, in ground laboratory accelerated tests, electrostatic charging of the PTFE target in high current/dose-rate laboratory electron beams can lead to deceleration and deflection of the incident electron beam, especially for lower energy electrons (Ref. 87). This effect needs to be considered when evaluating accelerated rate space simulation test results for insulating materials.

4.2.3.2. White Paint Thermal Control Coatings

Many satellite systems have used white paint thermal control coatings Z-93, YB-71, and S13GLO-1. As a result of a change in manufacturer of the potassium silicate binder/encapsulant material used in all

three paints, extensive requalification testing examined radiation stability of the newly reformulated versions of these paints, Z-93P, YB-71P, and S13GPLO-1, along with comparison to their predecessors (Refs. 55 and 88). In one of the tests (Ref. 88), samples were exposed to approximately 2600 equivalent UV sun hours along with 40 keV electrons at a flux of 6×10^{9} electrons/m^2s for a total fluence of 3×10^{16} electrons/m^2. Table 4 shows solar absorptance changes for original and reformulated white paints due to this testing.

This study proved a very important point regarding spacecraft materials degradation. Even seemingly minor changes in a material can produce significantly different vulnerability to radiation degradation. Radiation degradation of the white paint materials is very sensitive to impurity levels and processing conditions, so that even an "equivalent" chemical substitute for the potassium silicate binder did not produce a material with equivalent radiation durability. In fact, the YB-71P was found to be inadequately radiation stable to be space qualified, whereas Z-93P, using the same binder, was found to have adequate radiation stability to be considered space qualified (Ref. 88).

4.3. Mitigation of Radiation Degradation

In general, mitigation of radiation degradation of spacecraft materials is accomplished through careful material selection based on understanding radiation conditions for the mission and space ultraviolet and ionizing radiation durability of materials being considered. Where UV-vulnerable materials are necessary, some materials may be able to be protected through the use of protective coatings, such as the OCLI coating used on Tedlar® described in section 4.1.2.1. Although the OCLI coating was successfully used on Tedlar®, adhesion issues were observed when an OCLI coating was used on FEP, which will be described in section 5.2.3, so protection for one material may not be a guarantee of

successful protection application for another. Metallic coatings, such as vapor deposited aluminum (VDA), can generally protect vulnerable polymers from ultraviolet degradation, but processing defects, especially scratches or other types of line-shaped defects, may lead to local UV degradation. Additionally, metallic coatings and oxide coatings cannot provide significant protection from high energy ionizing radiation. In most cases, vulnerable materials, even with protective coatings, should be tested to the most conservative conditions to estimate their lifetime at mission conditions. It must be considered that radiation effects are often synergistic with thermal effects, which will be described in Section 5, and ground laboratory evaluations should consider all aspects of the space environment together.

5. Thermal and Thermal Cycling Effects

5.1. Environment Description

Earth orbital environments are capable of producing significant temperature variations as the spacecraft passes from sunlight to shadow. The number of thermal cycles expected for a mission depends upon the orbit. For example, spacecraft in low Earth orbit complete one orbit approximately every 90 minutes and spacecraft in geosynchronous orbit complete one orbit each Earth day (24 hours). The degree to which a material experiences thermal cycling depends upon its thermo-optical properties (solar absorptance and thermal emittance), its view of the Sun, its view of the Earth, its view of other surfaces of the spacecraft, durations of time in sun and in shadow, and the influence of equipment or components that produce heat.

5.2. Effects on Materials

On-orbit temperatures and thermal cycling pose a threat to materials durability for various reasons. First, for inhomogeneous materials in intimate contact with one another, such as in composites or coated

materials, a mismatch in coefficients of thermal expansion may lead to cracking or delamination when the material experiences significant temperature excursions. Second, mechanical properties of polymer materials can be a strong function of temperature (Ref. 89). This implies that during the course of on-orbit thermal cycling, a polymer may experience temperatures at which it has decreased strength or ductility making it more vulnerable to damage. Because radiation damage is generally more concentrated at the exposed surface of a material and diminishes through the thickness, one can consider that a radiation damaged polymer no longer has homogenous properties through its thickness, making it vulnerable to effects of a mismatch in coefficient of thermal expansion (CTE).

5.2.1. Effects on Composites

One report described results of an in-depth study of the effects of thermal cycling on composites for space applications including a carbon fiber-reinforced epoxy (ERL1962) and carbon fiber-reinforced cyanate ester (RS3) (Ref. 90). Variables in the study included thermal cycling temperature range, composite layer thickness, matrix type, and fiber type. It was found that cyanate ester matrix composites are more resistant to thermal cycling-induced microcracking than epoxy matrix composites. For carbon fiber epoxy matrix composites, the number of microcracks induced by thermal cycling reaches a saturation level as early as several hundred cycles, with many microcracks being observed after only a few thermal cycles. However, cyanate ester matrix composites show a threshold effect such that for less severe temperatures, thermal cycling does not cause any significant microcracking, and, for temperature ranges that do cause microcracking, a saturation level may be in the thousands of cycles. Also, composites with thinner laminate layers (50.8 μm) were found to be more susceptible to microcracking that composites with thicker layers (127 μm).

The Long Duration Exposure Facility provided opportunities to examine materials degradation due to space exposure in low Earth orbit for 69 months. Figure 19 shows an example of an apparent space thermal cycling-induced crack in an aluminum-chromium coating on a graphite epoxy panel that was located on the leading edge of LDEF. (Ref. 91) Atomic oxygen erosion of the graphite epoxy is also evident in the cracked area.

5.2.2. Effects on Spacecraft Paint Coatings

Z-93, a zinc oxide pigment/potassium silicate binder white paint applied to aluminum substrates, has been observed to microcrack upon thermal cycling (Ref. 92). This is an expected result of the CTE mismatch between the coating and the substrate. However, with proper substrate surface preparations, delamination and spalling arre prevented, so, despite a "mud-tiled" appearance due to microcracking, the painted surfaces exhibit durability to orbital thermal cycling. Anodized aluminum substrates can provide a less severe CTE mismatch for Z-93 and minimize the degree of microcracking (Ref. 92).

5.2.3. Synergistic Thermal, Thermal Cycling and Radiation Effects on Uncoated and Coated Teflon® FEP

Synergistic effects between radiation and thermal cycling have been observed for spacecraft materials in ground testing and in-space. In one test, thermal cycling was found to cause delamination and spalling of protective oxide coatings on FEP (Ref. 60). In this study, coatings examined included SiO_x (where x ~ 2) and a coating consisting of alternating layers of SiO_2, TiO_2, and Ta_2O_3 developed by OCLI. Samples were exposed to 5 kGy of 1 MeV electron radiation followed by thermal cycling, nominally in the range of -115 °C and 90 °C. Whereas some OCLI-coated samples that were not exposed to radiation and thermal cycling showed signs of minor coating adhesion problems, such as cracking and loss of coating in bent areas, spalling and delamination were observed only for samples which had been

exposed to both radiation and thermal cycling. An example of the effects of electron radiation and thermal cycling on the OCLI/FEP is shown in Figure 20. Severity of delamination and spalling was found to be worse for thicker coatings.

The VDA-coated 127 μm thick FEP outer most layer of the multilayer insulation blankets on the Hubble Space Telescope has become embrittled resulting in severe on-orbit cracking as shown in Figure 21. A sample of FEP retrieved during the second servicing mission (SM2), after 6.8 years in space, was significantly more embrittled than the same thickness FEP retrieved during the third servicing mission (SM3A), after 9.7 years in space. One of the differences in the environmental exposures between these samples was the maximum temperature exposure during thermal cycling. The retrieved SM2 insulation section curled after cracking, exposing the lower emittance back-surface aluminum to space. It was estimated that this extremely embrittled piece of insulation reached approximately 200 °C on-orbit, 150 °C higher than the nominal temperature extreme (–100 to 50 °C for solar facing FEP on HST). Several studies have been conducted to investigate the space environmental factors responsible for the degradation of FEP on the HST, including examinations of the combined effects of radiation and temperature or temperature cycling. A review board who investigated the severe FEP degradation on HST concluded that electron and proton radiation combined with on-orbit thermal cycling was necessary to cause the observed cracking of FEP on HST at areas of stress concentrations (Ref. 93).

One study examined the differences in degradation produced by the space environment and ground testing intended to replicate exposure conditions for FEP on the Hubble Space Telescope. (Ref. 94) Samples of 127 μm FEP film were exposed to 0.5 MeV electrons and 1 MeV protons to provide fluences equivalent to those of various HST exposure durations up to 20 years. This radiation exposure

was followed by thermal cycling in the temperature range of -100 °C to + 50 °C, the nominal range for the FEP exterior layer of thermal insulation on HST. Thermal cycling was conducted in a nitrogen purged chamber at a nominal rate of 4 cycles per minute. Effects of these exposures compared to HST exposures on strength and elongation of FEP are shown in Figure 22. It is evident that laboratory testing severely underpredicted the on-orbit degradation caused by HST exposure of FEP for even 3.6 years, where laboratory exposures equivalent to 20-40 years in space were required for similar degradation. The data point for SM2 (6.8 yr) in Figure 22, near zero elongation, is shown for reference; however, as described above, this FEP sample was exposed to an upper temperature limit of ~ 200 °C, much higher than the nominal FEP materials on HST which reach 50 °C.

Research has been conducted to determine the effects of heating on irradiated FEP in order to better understand the effect of temperature on the rate of degradation, and on the mechanism of degradation of FEP insulation in the LEO environment. In one study, samples of pristine FEP, x-ray irradiated FEP, and FEP retrieved from HST were heated from 50 to 200 °C at 25°C intervals in a high vacuum furnace and evaluated for changes in tensile properties and density (Ref. 95). Even though the ground-laboratory x-ray exposure (conducted at room temperature) provided an areal dose (D, the total energy absorbed per unit area integrated through the full thickness in FEP that was orders of magnitude higher than the HST on-orbit areal dose, it did not produce the extent of damage observed for the HST-exposed FEP. However, the laboratory exposure provided sufficient degradation to show the effects of subsequent heating on irradiated FEP. This study found that heating did not embrittle non-irradiated FEP Teflon; however, there was a significant dependence of the embrittlement of irradiated FEP on heating temperature, with near complete loss of elongation at failure at 100 °C and higher. These results are shown in Figure 23.

This and other studies (Ref. 96) support the conclusion that radiation (solar, x-ray, particle radiation) induced chain scission is the primary mechanism of embrittlement of FEP on HST, and indicate the significant impact of the on-orbit temperature of FEP with respect to its degradation in the space environment.

One study examined candidate materials to replace the degrading outer layer of aluminized FEP on HST. Candidate materials that were considered are indicated in Table 5. Various sets of these candidate replacement materials were exposed to combinations of electron/proton radiation, atomic oxygen, soft x-rays, thermal cycling and near ultraviolet radiation at various facilities in order to evaluate their HST on-orbit durability (Refs. 97 and 98). Two sets of samples (B1 and M2) previously exposed to charged particle radiation were exposed to soft x-rays and one sample set (B1) was also thermal cycled under load. Thermal cycling temperatures ranged between -100 °C and +50 °C and spring loading provided stress on each sample of approximately 12.4 MPa. Samples received 1000 thermal cycles. Thermal cycled samples are shown in Figure 24. Metallized 5 mil thick FEP samples B1.2 and B1.4, shown in Figure 24a, with fiberglass scrims and Kapton® substrates, tore in half during thermal cycling under load. (Ref. 97) This may be attributed to the low tear resistance of Kapton®. These samples performed worse that Sample B1.8, shown in Figure 24b, the current HST MLI material (5 mil thick aluminized-FEP), which tore about 90 percent of the width during thermal cycling. Tear propagation of the B1 samples was attributed to thermal cycling under a high load. The prior radiation exposures did not appear to have an additional effect on tearing, and no tearing occurred due to mechanical load cycling. Following the evaluation of all test results, 5 mil FEP/Al/adhesive/Nomex® scrim was recommended as replacement material for the outer thermal blanket layer for HST (Ref. 98).

Ground-based environmental durability tests, such as that discussed in reference 94, indicate that exposing materials in accelerated tests to environmental model predicted spacecraft mission exposures of UV and/or ionizing radiation sources does not simulate the extent of damage that occurs in the space environment. One approach to overcoming the difficulties in simulating the space environment using ground-based testing is to calibrate the facility using data from actual space exposed materials to determine exposure levels required to replicate degraded properties observed in space. Reference 99 describes a ground-to-space correlation method that uses a multiple step process to determine the durability of expanded-polytetrafluoroethylene (ePTFE) for International Space Station (ISS) applications based on ground-based x-ray irradiation and heating exposure that simulates bulk embrittlement as occurs in fluorinated ethylene propylene (FEP) thermal insulation covering the Hubble Space Telescope (HST). This method was designed to damage the back surface of equivalent thickness ePTFE to the same amount of scission damage as occurred in HST FEP (based on elongation data) and then correct for differences in ground test ionizing radiation versus space radiation effects, temperature variations, space ionizing radiation environment variations (spacecraft altitude, inclination and duration), and thickness variations.

6. Micrometeoroid and Orbital Debris Effects

6.1. Environment Description

Micrometeoroids are of extraterrestrial origin and as such will have a flux which is reasonably constant with time. Their velocity is typically in the 4 to 51 km/sec range (Refs. 100 and 101) with average velocity near 20 km/sec. As shown in Figure 25, as micrometeoroid particle size decreases, the

flux of particles increases. Orbital debris is of man-made origin as a result of spent solid rocket booster exhaust, Satellite breakups or other man-caused origins. Orbital debris has an average velocity of 8.7 km/sec (Ref. 102). Because of the man made origin and atmospheric drag, orbital debris flux is highly dependent upon the world's spacecraft launch frequency and occurrences of orbital breakups. The orbital debris size distribution can also be seen in Figure 25. The Micrometeoroid Flux Model shown in Figure 25 was developed based on the Cour-Palais model (Ref. 103), and the Debris Flux Model was developed based on the Kessler model (Ref. 104). The combined occurrence of micrometeoroids and orbital debris is non-uniform around a spacecraft which is fixed in orientation relative to the ram direction. Figure 26 shows a polar plot of the number of impacts around the LDEF which was in LEO for 5.75 years "in a fixed orbital orientation" (Ref. 105).

6.2. Interactions with Materials

The impact of micrometeoroid or orbital debris with spacecraft materials is usually sufficiently energetic to cause vaporization of the impacting particle as well as produce an impact crater of volume an order of magnitude greater than the impacting particle. For example, the kinetic energy of an aluminum particle traveling at 6 km/sec is sufficient to vaporize aluminum to form a crater that is roughly 5 times the diameter of the incoming particle (Ref. 106). Figure 27 shows scanning electron microscope photographs of typical hypervelocity impact craters in aluminum and fluorinated ethylene propylene (FEP) Teflon® from the LDEF spacecraft (Ref. 107). The violence of the microscopic explosive vaporization can cause delamination in layered materials as shown in Figure 28, which shows a layered structure of FEP, silver, and Z306 black paint flown on LDEF that was delaminated over a diameter order of magnitude greater than the impacting particle followed by subsequent atomic oxygen oxidation of the underlying silver (Ref. 108). The ejection of impact crater material can be a source of spacecraft self-contamination. Large particle impacts, although rare in occurrence, have the potential to

penetrate pressure vessels or cause structural damage. The largest impact crater on the LDEF spacecraft was 5.7 mm in diameter. (Ref. 109).

6.3. Mitigation Techniques

Localized damage caused by micrometeoroid or orbital debris impacts on spacecraft surfaces can be mission threatening if the impact occurs on electrical wires, power cables or pressure vessels. Reduction in the probability of catastrophic loss in an electrical power conductor can be achieved through use of a ladder configured conductor rather than a single conductor. The concept is that one would divide the current into two smaller conductors that are separated with occasional rung conductors that could carry current back and forth across the two main long conductors in case one conductor was severed by hypervelocity impact. Only a short length of single conductor between the rungs on either side of impact breakage site would have to carry twice the normal current.

Mitigation techniques for power cables can simply be the use of redundant separated cables so that the probability of all cables failing is acceptably small. The same technique is applicable to electrical signal conductors. Such techniques are simple to accomplish in flat ribbon conductors that are laminated with polymer insulation.

Because one micrometeoroid or debris impact can cause total loss in pressure of a tank or container that can fail a mission or cause loss of life for manned missions mitigation techniques are important. The technique used to prevent penetration of pressure vessels has been to add an outer thin wall, often called a "Whipple shield", to cause the impacting particle to break up upon impact (Refs. 110 and 111). The debris from the impact then spreads over a large area on the surface of the pressure vessel which is spaced concentrically inside the shield material. Because the debris is spread over a large area, its ability to penetrate the inner critical chamber is greatly reduced. Variants of this concept for

structured projection of tubular structures include filling the space between two sides of a tubular structure with low density ceramic fiber fill which also acts to absorb the energy of the broken up primary impact debris (Ref. 111). Damage to the back wall of the structure is prevented by the energy absorbing fill material.

7. Concluding Remarks

Spacecraft materials exposed to Earth orbit environments have been found to undergo degradation or damage due to environmental threats including atomic oxygen, contamination, radiation, temperature effects and temperature cycling, and micrometeoroids and orbital debris. The degree to which the space environment degrades or damages materials depends upon the unique conditions of an individual spacecraft environment and the susceptibility of the material to being altered by these environmental exposures. As has been shown in this chapter, space environment interactions with materials are complex, often producing combined or synergistic effects. Accurately predicting the behavior of materials in these complex space environments is important to the success of space missions yet can be difficult to accomplish.

Since the first Space Shuttle flights, significant advancements have been made in understanding atomic oxygen effects on materials, namely, in quantifying atomic oxygen degradation for many polymers, in development of coatings to prevent atomic oxygen degradation, in development of calibrated laboratory simulation methods, and in development of modeling tools to predict in-space degradation. However, for radiation effects and synergistic effects with temperature, accelerated testing in the laboratory using individual or combined environments to estimated mission exposure fluences or doses has been generally unable to accurately replicate damage observed in space. Furthermore, complex differences

between the space and laboratory environments require cautious interpretation of results. These complications of predicting durability of spacecraft materials has led to efforts in developing ground-to-space correlation methods for radiation durability testing, for example, exposing Teflon® materials to exposures based on the dose of radiation that produces reduction in FEP mechanical properties equivalent to that observed in space, rather than to actual mission fluence exposures.

As space missions are becoming longer in duration and require lighter weight materials with specially tailored properties, it is critical that advancements continue in understanding material degradation mechanisms and in the development of simulation laboratory durability testing and modeling capabilities. This is crucially dependent on the retrieval and subsequent testing of long duration space exposed materials, such as the MISSE flight experiment. These advancements will assure accuracy in predicting long-term material durability in the space environment for future missions.

References

1	Dickerson R.E, Gray H.B., & Haight G.P., Chemical Principles 3rd Edition, Benjamin Cummings Publishing Co. Inc. Menlo Park, CA, 1979, p. 457.
2	NOAA, NASA and USAF, U.S. Standard Atmosphere, 1976, NASA Tech. Memo TMX-74335, 1976
3	Banks B.A., Rutledge S.K., de Groh K.K., "Low Earth Orbital Atomic Oxygen, Micrometeoroid, and Debris Interactions with Photovoltaic Arrays" Presented at the 11th Space Photovoltaic Research and Technical Conference (SPRAT XI) NASA Lewis Research Center, Cleveland, OH, May 7-9, 1991.
4	Hedin A.E., "MSIS-86 Thermospheric Model", Journal of Geophysical Research, Vol. 92, 1987, p. 4649.
5	de Groh K.K. and Banks B.A. "Atomic Oxygen Undercutting of Long Duration Exposure Facility Aluminized-Kapton Multilayer Insulation", Journal of Spacecraft and Rockets (AIAA), Vol. 31, No. 4, July-August 1994, pp 656-664.
6	Banks B.A., de Groh K.K., Rutledge S.K., and DiFilippo F.J., "Prediction of In-Space Durability of Protected Polymers Based on Ground Laboratory Thermal Energy Atomic Oxygen", Protection of Materials and Structures form the Low Earth Orbit Space Environment, Eds. Kleiman J.I. and Tennyson R.C. Kluwer Academic Publishers, Netherlands, 1999, pp 89-100.
7	Banks B.A., Rutledge S.K., Auer B.M. and DiFilippo, F.J., "Atomic Oxygen Undercutting of Defects on SiO2 Protected Polyimide Solar Array Blankets", Materials Degradation in Low Earth Orbit, Eds. Srinivasan V. and Banks B. TMS, 1990, pp. 15-33.
8	Mende S.B., Swenson G.R., and Clifton K.S., Science, Vol. 225:191, 1984.
9	Rice C.J., Russell R.W., "Infrared Spectral Measurement of Space Shuttle Glow", Geophysical Research Letters, 19(10), 22 May, 1992, pp 989-992.
10	Caledonia, G.E., "Laboratory Simulations of Energetic Atom Interactions Occuring in Low Earth Orbit", Rarefied Gas Dynamics: Space Related Studies, Eds. Munts E.O., Weaver D.P., Campbell D.H., Vol. 116, Progress in Astronautics and Aeronautics, AIAA, 1989, pp. 129-142.
11	Mata, A., Su, X., Fleischman, A., Banks, B., Miller, S., and Midura, R., "Osteoblast Attachment to a Textured Surface in the Absence of Exogenous Adhesion Proteins", IEEE Transactions on Nanobioscience, Vol. 2, No. 4, December 2003.
12	Banks, B.A., Rutledge S.K., "Low Earth Orbital Atomic Oxygen Simulation for Materials Durability Evaluation", Fourth European Symposium on Spacecraft Materials in Space Environment, Toulouse, France, 6-9, September, 1988, pp.372-392.
13	Leger L.J., "Oxygen Atom Reaction With Shuttle Materials at Orbital Altitudes -Data and Experiment Status", AIAA-83-0073, January, 1983.
14	Bruce A. Banks, S. K. Rutledge, Phillip E. Paulsen and Thomas J. Steuber, "Simulation of the Low Earth Orbital Atomic Oxygen Interaction With Materials by Means of an Oxygen Ion Beam," Presented ast the 18th Annual Symposium on Applied Vacuum Science and Techcnology, Clearwater Beach, Florida, February 6-8, 1989; NASA TM 101971, 1989.
15	Bruce A. Banks, "The Use of Fluoropolymers in Space Applications" in *Modern Fluoropolymers*, Edited by John Scheirs, (pp.103-113), Chapter 4, John Wiley & Sons Ltd, 1997.
16	"Prediction of Erosion of Polymer-Based Materials by Atomic Oxygen in LEO," Integrity testing Laboratory Inc. Final Report, GRC Contract #C-72917-G, 1998.
17	Kleiman, J., Iskanderova, Z., Banks, B. A., de Groh, K. K., and Sechkar, E. A., Proceedings of the 8th International Symposium on Materials in a Space Environment, Arcachon, France, June 5-9, 2000.
18	K. K. de Groh, B. A. Banks, A. M. Hammerstrom, E. E. Youngstrom, C. Kaminski, L. M. Marx, E. S. Fine, J. D. Gummow and D. Wright, "MISSE PEACE Polymers: An

	International Space Station Environmental Exposure Experiment," Proceedings of the Conference on ISS Utilization - 2001, October 15-18, 2001, Cape Canaveral, Fl. AIAA #2001-4923; also NASA TM-2001-211311, November 2001.
19	Banks B.A., de Groh K.K., Rutledge S.K., and Haytas, C.A., "Consequences of Atomic Oxygen Interaction with Silicone and Silicone Contamination on Surfaces in Low Earth Orbit", 44th Annual Meeting sponsored by the International Society for Optical Engineering, Denver, Colorado, July 21, 1999. NASA TM-1999-209179.
20	de Groh K., McCollum T., "Low Earth Orbital Durability of Protected Silicones for Refractive Photovoltaic Concentrator Arrays", Journal of Spacecraft and Rockets, Vol. 32:1, Jan.-Feb., 1995.
21	Banks B.A., de Groh K., Rutledge S., and DiFilippo F., "Prediction of In-Space Durability of Protected Polymers Based on Ground Laboratory Thermal Energy Atomic Oxygen", presented at the 3rd International Conference for Protection of Materials and Structures from Low Earth Orbit Space Environment, University of Toronto Institute for Aerospace Studies, Toronto, Canada, April 25-26, 1996, NASA TM-107209.
22	Banks B., Miller S., de Groh K., Chan A., Sahota M., "The Development of Surface Roughness and Implications for Cellular Attachment in Biomedical Applications", Materials Research Society 2001 Fall Meeting, Boston, Massachusetts, November 26-30, 2001, NASA TM-2001-211288.
23	de Groh K.K., Banks B.A. and Smith D.C., "Environmental Durability Issues for Solar Power Systems in Low Earth Orbit," Solar Engineering 1995, Volume 2, pp. 939-950; NASA TM 106775, March 1995.
24	Banks B.A., Rutledge S.K., de Groh K.K., Mirtich M.M., Gebauer L., Olle R., and Hill C., "The Implications of the LDEF Results on Space Station Freedom Power System Materials", 5th International Symposium on Materials in a Space Environment, Cannes-Mandelieu, France, September 16-20, 1991.
25	Banks B.A., Mirtich M.J., Rutledge S.K., Swec D.M. and Nahra H.K., "Ion Beam Sputter-Deposited Coatings for Protection of Spacecraft Polymers in Low Earth Orbit", 23rd Aerospace Sciences Meeting (AIAA), Reno, Nevada, January 14-17, 1985, NASA TM-87051.
26	Silverman E.M., "Space Environmental Effects on Spacecraft: LEO Materials Selection Guide", NASA Contractor Report 4661 Part 2, August, 1995, Section 10-38.
27	Banks B.A., Mirtich M.J., Rutledge S.K., Swec D.M., "Sputtered Coatings for Protection of Spacecraft Polymers", 11th International Conference on Metallurgical Coatings (AVS), San Diego, California, April 9-13, 1984, NASA TM-83706.
28	Dever J.A., Rutledge S.K., Hambourger P.D., Bruckner E., Ferrante R., Pal A.M., Mayer K., Pietromica A.J., "Indium Tin Oxide-Magnesium Fluoride Co-Deposited Films for Spacecraft Applications", International Conference on Metallurgical Coatings (AVS), San Diego, California, April 24-26, 1996, NASA TM-1988-208499.
29	Banks B.A., Snyder A., Miller S.K., Demko R., "Issues and Consequences of Atomic Oxygen Undercutting of Protected Polymers in Low Earth Orbit", 6th International Conference on Protection of Materials and Structures from Space Environment, Toronto, Canada, May 1-3, 2002, NASA TM-2002-211577.
30	Rutledge, S.K., Mihelcic J.A., "The Effect of Atomic Oxygen on Altered and Coated Kapton Surfaces for Spacecraft Applications in Low Earth Orbit", Materials Degradation in Low Earth Orbit, Eds. Srinivasan V. and Banks B. TMS, 1990, pp. 35-48.
31	Goode D.C., Williams A.W., Wood N.J., Binzakaria A., "Photothermal Imaging of Gold and Vermiculite Coated Kapton Exposed to Atomic Oxygen", ESA Proceedings of the 6th International Symposium on Materials in a Space Environment, Nov. 1994, SEE N95-27568 09-23, pp 201-206.
32	Rutledge S.K., Olle R.M., "Space Station Freedom Solar Array Blanket Coverlay Atomic Oxygen Durability Testing Results", Proceedings of the 38th International SAMPE Symposium, May 10-13, 1993, pp 679-693.

33	Banks B., Stueber T., and Norris M., "Monte Carlo Computational Modeling of the Energy Dependence of Atomic Oxygen Undercutting of Protected Polymers," 4th International Space Conference ICPMSE-4, Toronto, Canada, April 23-24, 1998, NASA TM-1998-207423.
34	Banks B.A., Auer B.M., Rutledge S.K., Gebauer L. and Sechkar E.A., "Monte Carlo Modeling of Atomic Oxygen Interaction with Protected Polymers for Projection of Materials Durability in Low Earth Orbit", Proceedings of the MRS 1992 Spring Meeting, San Francisco, California, April 27-May 1, 1992.
35	Banks B.A. and Stueber T.J., "Monte Carlo Computational Techniques for Prediction of Atomic Oxygen Erosion of Materials", Proceedings of the NATO Advanced Research Workshop on Computer Modeling of Electronic and Atomic Processes in Solids, Wroclaw, Poland, May 20-23, 1996, Eds. Tennyson R.C. and Kiv A.E., Kluwer Academic Publishing, 1997.
36	Banks B.A., Miller S.K.R., de Groh K.K., Demko R., "Scattered Atomic Oxygen Effects on Spacecraft Materials", Proceedings of the 9th International Symposium on Materials in a Space Environment, Noordwijk, The Netherlands, June 16-20, 2003, ESA SP-540, pp. 145-152.
37	D. A. Jaworske, K. K. de Groh, G. Podojil, T. McCollum and J. Anzic, "Leveling Coatings for Reducing the Atomic Oxygen Defect Density in Protected Graphite Fiber Epoxy Composites," Journal of the IES (Institute of Environmental Sciences), May/June 1994, Vol. XXXVII, No. 3, pp. 26-31.
38	K. K. de Groh, T. M. Dever and W. F. Quinn, "The Effect of Leveling Coatings on the Atomic Oxygen Durability of Solar Concentrator Surfaces," NASA TM 102557, April 1990.
39	Iskanderova Z.A., Kleiman J.I., Gedimenko Y., Morrison W.D., Tennyson R.C., "Surface Modification of Polymer-Based Materials by Ion Implantation-A New Approach for Protection in LEO", Protection of Materials and Structures for the Low Earth Orbit Space Environment, Eds. Kleiman J.I. and Tennyson R.C., Kluwer Academic Publishers, Netherlands, 1999, pp 225-234.
40	Rutledge S.K., Cooper J.M., and Olle R.M., "The Effect of Atomic Oxygen on Polysiloxane-Polyimide for Spacecraft Applications in Low Earth Orbit" Proceedings of the 4th Annual Workshop on Space Operations Applications and Research (SOAR '90), Albuquerque, New Mexico, June 26-28, 1990, NASA CP 3103 Vol. II, pp. 755-762.
41	Gonzalez R.I., Tomczak S.J., Minton T.K., Brunsvold A.L., Hoflund G.B., "Synthesis and Atomic Oxygen Erosion Testing of Space-Survivable POSS (Polyhedral Oligomeric Silsesquioxane) Polyimides", Proceedings of the 9th International Symposium on Materials in a Space Environment, Noordwijk, The Netherlands, June 16-20, 2003, ESA SP-540, pp. 113-120.
42	Illingsworth M.L., Betancourt L., He L., Chen Y., Terschak J.A., Banks B.A., Rutledge S.K., Cales M., "Zr-Containing 4,4'-ODA/PMDA Polyimide Composites", NASA TM-2001-211099, 2001.
43	Shepp A., Haghighat R., Lennhoff J., Schuler P., Connell J., St. Clair T., Vaughn J., and Swiener J., "TOR and COR AO-VUV Resistant Polymers for Space", Protection of Materials and Structures for the Low Earth Orbit Space Environment, Eds. Kleiman J.I. and Tennyson R.C., Kluwer Academic Publishers, Netherlands, 1999, pp 235-254.
44	Chen, P. T., "Contamination Effects due to Space Environmental Interactions," American Institute of Aeronautics and Astronautics, AIAA Paper No. 2001-0095, January 2001
45	Walter, N. A. and Scialdone, J. J., "Outgassing Data for Selecting Spacecraft Materials," National Aeronautics and Space Administration, NASA Reference Publication 1124, Revision 4, June 1997.
46	A. C. Tribble, The Space Environment: Implications for Spacecraft Design, Princeton University Press, Princeton, NJ, 1995.

47	Noter Y., Grossman E., Genkin L., Haruvy Y., Murat M., Ross I., Vered R., Lifshitz Y., Efraty Y., Granot H., Halbersberg A., Luria H., and Stoler A., "Variations in the Telemetry of an Offeq Satellite's Sun Sensors", presented at the 3rd International Space Forum on Protection of Materials and Structures from Low Earth Orbit Space Environment, University of Toronto Institute for Aerospace Studies, Toronto, Canada, April 25-26, 1996.
48	Tribble, A. C., Boyadjian, B., Davis, J., Haffner, J., and McCullough, E., "Contamination Control Engineering Design Guidelines for the Aerospace Community," National Aeronautics and Space Administration, NASA Contractor Report 4740, May 1996.
49	American Society for Testing and Materials ASTM-E 490-73a (Reapproved 1992), "Solar Constant and Air Mass Zero Solar Spectral Irradiance Tables."
50	Koller, L. R., Ultraviolet Radiation, John Wiley & Sons, NewYork, 1965.
51	Schnabel, W., Polymer Degradation: Principles and Practical Applications, Macmillan Publishing Co., Inc., New York, 1981, Chapter 4.
52	Adams, M. R., "The Degradation of Polymeric Spacecraft Materials by Far-UV Radiation and Atomic Oxygen," UMI Dissertation Services, Ann Arbor, MI, 1993, p. 138?
53	Dever, J. A., Pietromica, A. J., Stueber, T. J., Sechkar, E. A., Messer, R. K., "Simulated Space Vacuum Ultraviolet (VUV) Exposure Testing for Polymer Films," AIAA Paper No. 2001-1054, American Institute of Aeronautics and Astronautics, January 2001.
54	Gatto, A., Escoubas, L., Roche, P., Comandré, M., "Simulation of the Degradation of Optical Glass Substrates caused by UV Irradiation while Coating," Optics Communications 148 (1998), pp. 347-354.
55	Harada, Yoshiro and Deshpande, Mukund, "Requalification of White Thermal Control Coatings," Wright Laboratory Report No. WL-TR-94-4126, October 1994.
56	McKellar, J. F. and Allen, N. S., Photochemistry of Man-made Polymers, Applied Science Publishers Ltd., London, 1979, p. 31.
57	Grossman, E., Noter, Y., and Lifshitz, Y., "Oxygen and VUV Irradiation of Polymers: Atomic Force Microscopy (AFM) and Complimentary Studies," in Proceedings of the 7th International Symposium on Materials in Space Environment,Toulouse, France, 16-20 June 1997, Published by ESA, Noordwijk, Netherlands, pp. 217-22.
58	Skurat, V. E., Barbashev, E. A., Budashov, I. A., Dorofeev, Yu. I., Nikiforov, A. P., Ternovoy, A. I., Van Eesbeek, M., and Levadou, F., "The Separate and Combined Effects of VUV Radiation and Fast Atomic Oxygen on Teflon FEP and Silicon Carbide," in Proceedings of the 7th International Symposium on Materials in Space Environment, Toulouse, FRANCE, 16029 June 1997, Noordwijk, Netherlands, ESA, 1997, pp. 267-279
59	Dever, J. A., and McCracken, C. A., "Effects of Various Wavelength Ranges of Vacuum Ultraviolet Radiation on Teflon FEP Film" in Proceedings of the 9th International Symposium on Materials in a Space Environment, European Space Agency, ESA SP-540, September 2003, pp. 367-373.
60	Joyce Dever and Kim de Groh, "Vacuum Ultraviolet Radiation and Atomic Oxygen Durability Evaluation of HST Bi-Stem Thermal Shield Materials," NASA/TM-2002-211364, February 2002.
61	Jukeikis, H. S. "Space Radiation Effects on Teflon Films," Report SAMSO-TR-79-070, The Aerospace Corporation, September 1979.
62	Toupikov, , V. I., Khatipov, S. A., Charniavsky, A. I., and Stepanov, V. F., "Degradation of Mechanical and Electrophysical Properties of Teflon FEP Films Under Combined Action of Far Ultraviolet and Thermal Cycling," Proceedings of the 7th International Symposium on Materials in Space Environment, Toulouse, FRANCE, 16029 June 1997, Noordwijk, Netherlands, ESA, 1997, pp. 77-85.
63	DuPont, Technical Information on Tedlar (Polyvinyl fluoride film), http://www.dupont.com/tedlar/, 2003.
64	Stuckey, W. K.; Meshishnek, M. J., "Space Environmental Stability of Tedlar with Multi-Layer Coatings: Space Simulation Testing Results," Aerospace Corp., Report No.: AD-A387139; TR-2000(85665)-8; SMC-TR-00-03 under Contract No.: F04701-93-C-0094, El

	Segundo, CA., Aug. 20, 2000.
65	Grossman, E.; Noter, Y.; Lifshitz, Y., "Oxygen and VUV irradiation of polymers - Atomic force microscopy (AFM) and complementary studies," in Proceedings of the 7th International Symposium on Materials in Space Environment, Toulouse, France, June 16-20, 1997, Noordwijk, Netherlands, ESA, 1997, p. 217-223.
66	Seki, K., Tanaka, H., and Ohta T., "Electronic Structure of Poly(tetrafluoroethylene) Studied by UPS, VUV Absorption, and Band Calculations," Physica Scripta, vol. 41, 1990, pp. 167-171.
67	Joyce A. Dever, Russell Messer, Charles Powers, Jacqueline Townsend, and Eve Wooldridge, "Effects of Vacuum Ultraviolet Radiation on Thin Polyimide Films," High Performance Polymers, Vol. 13, No. 3, Sept. 2001, pp. S391-399.
68	Luoma, G. A, Rowland, R. D., "The Effects of Sunlight and Humidity on CF-188 Composite Resin" Defence Research Establishment Pacific Technical Memorandum 89-07, April 1989.
69	Liau, W. B., Tseng, F. P., "Effect of Long-Term Ultraviolet Light Irradiation on Polymer Matrix Composites," Polymer Composites, Vol. 19, No. 4, p. 440-445, 1998.
70	Silverman, Edward M., "Space Environmental Effects on Spacecraft: LEO Materials Selection Guide," Prepared for Langley Research Center under Contract No. NAS1-19291, NASA Contractor Report 4661 Part 1, August 1995.
71	Holmes-Siedle, Andrew and Adams, Len, Handbook of Radiation Effects, Oxford University Press, New York, 2002.
72	Hastings, Daniel and Garrett, Henry, Spacecraft-Environment Interactions, Cambridge University Press, New York, 1996.
73	Website of the National Oceanic and Atmospheric Administration's Space Environment Center, Primer on Space Weather, http://www.sec.noaa.gov/primer/primer.html.
74	Website of the National Oceanic and Atmospheric Administration's National Geophysical Data Center, Space Physics Interactive Data Resource, http://spidr.ngdc.noaa.gov/spidr.
75	Dever, J. A., de Groh, K. K., Banks, B. A., Townsend, J. A., Barth J., L., Thomson, S, Gregory, T., Savage, W., "Environmental Exposure Conditions for Teflon FEP on the Hubble Space Telescope,"High Performance Polymers, 12, No.1, March 2000, pp. 125-139
76	Barth, Janet L., "Space and Atmospheric Environments: From Low Earth Orbits to Deep Space," in Proceedings of the 9th International Symposium on Materials in a Space Environment, European Space Agency, ESA SP-540, September 2003, pp. 17-30.
77	Sawyer, D. M., Vette, J. I., "AP-8 Trapped Proton Environment for Solar Maximum and Solar Minimum," NSSDC/WDC-A-R&S, 76-06, NASA/Goddard Space Flight Center, Greenbelt, MD, December 1976.
78	Vette, J. I., "The AE-8 Trapped Electron Model Environment," NSSDC/WDC-A-R&S 91-24, NASA/Goddard Space Flight Center, Greenbelt, MD, November 1991.
79	Schnabel, W., Polymer Degradation: Principles and Practical Applications, Macmillan Publishing Co., Inc., New York, 1981, Chapter 5.
80	Holmes-Siedle, Andrew and Adams, Len, Handbook of Radiation Effects, Oxford University Press, New York, 2002, p. 568-570.
81	Stuckey, W. K. and Meshishnek, M. J., "Solar Ultraviolet and Space Radiation Effects on Inflatable Materials," in Jenkins, C. H. M., ed., Gossamer Spacecraft: Membrane and Inflatable Structures Technology for Space Applications, Volume 191, Progress in Astronautics and Astronautics, American Institute of Aeronautics and Astronautics, Reston, Virginia, 2001, pp. 303-320.

82	K. K. de Groh and J. D. Gummow, "Effect of Air and Vacuum on the Tensile Properties of X-ray Exposed Aluminized-FEP," HPP Vol. 13, No. 3, Sept. 2001, pp. S421-S431.
83	Russell, D. A., Connell, J. W., Fogdall, L. B., "Electron, Proton, and Ultraviolet Radiation Effects on Thermophyisical Properties of Polymeric Films," *Journal of Spacecraft and Rockets*, Vol. 39, No. 6, Nov.-Dec. 2002, pp. 833-838.
84	Joyce Dever, Charles Semmel, David Edwards, Russell Messer, Wanda Peters, Amani Carter and David Puckett, "Radiation Durability of Candidate Polymer Films for the Next Generation Space Telescope Sunshield," AIAA 2002-1564, April 2002.
85	Laghari, J. R., and Hammoud, A. N., "A Brief Survey of Radiation Effects on Polymer Dielectrics," *IEEE Transactions on Nuclear Science,* Vol. 37, No. 2, April 1990, pp. 1076-1083.
86	Harrison, S. E., "A study of gamma ray photoconductivity in organic dielectric materials," Sandia Corporation, Report No. SCDC-2580, 1962.
87	S. L. Koontz, J. L. Golden, M. J. Lorenz, M. D. Pedley, "Ionizing Radiation Effects on ISS ePTFE Jacketed Cable Assembly" Proceedings of the 9th International Symposium on Materials in a Space Environment, Noordwijk, The Netherlands, June 16-20, 2003, ESA SP-540 (Sept. 2003) pp. 297-301.
88	Meshishnek, M. J., Hemminger, C. S., and Gyetvay, S. R., "Space Environmental Exposure of IITRI White Thermal Control Paints," Aerospace Corporation, Report No. TR-95(5904)-2, April 27, 1995.
89	Reed, R. P., Schramm, R. E., and Clark, A. F., "Mechanical, Thermal, and Electrical Properties of Selected Polymers," *Cryogenics*, Vol. 13, February 1973, pp. 67-82.
90	Brown, Timothy L., "Microcracking of Materials for Space," PhD Dissertation, Virginia Polytechnic Institute and State University, Oct. 1998. Also, Final Report for Grant NAG-1-1912, NASA Langley Research Center, October 1998.
91	K.K. de Groh, B. A. Banks and D. C. Smith, "Environmental Durability Issues for Solar Power Systems in Low Earth Orbit," Solar Engineering 1995, Volume 2, pp. 939-950; also NASA TM 106775, March 1995.
92	Daneman, S. A., Babel, H. W., Hasegawa, M. M., "Selection Rationale, Application, Optical Properties, and Life Verification of Z-93 for the Space Station," McDonnell Douglas Aerospace, Report No. 94H0632, August 1994.
93	Townsend, J. A., Hansen, P. A., Dever, J. A., de Groh, K. K., Banks, B. A., Wang, L., He, C., "Hubble Space Telescope metallized Teflon FEP thermal control materials: on-orbit degradation and post-retrieval analysis," High Performance Polymers, 11, No. 1, March 1999, pp. 81-100.
94	Townsend, J., Powers, C., Viens, M., Ayres-Treusdell, M., and Munoz, B., "Degradation of Teflon FEP Following Charged Particle Radiation and Rapid Thermal Cycling," in Proceedings of the 20th Space Simulation Conference: The Changing Testing Paradigm, National Aeronautics and Space Administration, CR-1998-208598, October 1998, pp. 201-209.
95	de Groh, K. K.,and Martin, M., "The Effect of Heating on the Degradation of Ground Laboratory and Space Irradiated Teflon FEP," National Aeronautics and Space Administration, TM-2002-211704, July 2002.
96	de Groh, K. K., Dever, J. A., Sutter, J. K., Gaier, J. R., Gummow, J., D., Scheiman, D. A. and He, C., "Thermal contributions to the degradation of Teflon FEP on the Hubble Space Telescope, Proceedings of the 46th International SAMPE Symposium and Exhibition, Long Beach, CA, May 6-10, 2001. Book 2 ; Covina, CA, Society for the Advancement of Material and Process Engineering (Science of Advanced Materials and Process Engineering Series. Vol. 46), 2001, p. 1826-1840.
97	K.K. de Groh, B. A. Banks, E. A. Sechkar and D. A. Scheiman, "Simulated Solar Flare X-Ray and Thermal Cycling Durability Evaluation of Hubble Space Telescope Thermal Control Candidate Replacement Materials," Presented at the 4th ICPMSE Conference, Toronto, Canada, April 23-24, 1998; NASA TM-1998-207426, December 1998.

98	J. A. Townsend, P. A. Hansen, M. W. McClendon, K. K de Groh and B. A. Banks, "Ground-based testing of replacement thermal control materials for the Hubble Space Telescope," Special Issue: High Perform. Polym 11 (1999) 63-79.
99	K. K. de Groh, B. A. Banks, J. A. Dever and J. C. Hodermarsky, "Use of Hubble Space Telescope Degradation Data For Ground-Based Durability Projection of ePTFE on ISS," Proceedings of the 9th International Symposium on Materials in a Space Environment, Noordwijk, The Netherlands, June 16-20, 2003, ESA SP-540 (Sept. 2003) pp. 281-290.
100	Kinard W.H., Martin G.D., "Long Duration Exposure Facility (LDEF) Space Environments Overview", Proceedings of the LDEF-69 Months in Space First Post-Retrieval Symposium, Kissimmee, Florida, June 2-8, 1991, NASA CP-3134 Part 1, pp 49-60
101	Zook H.A., "Deriving the Velocity Distribution of Meteoroids from the Measured Meteoroid Impact Directionality on the Various LDEF Surfaces", Proceedings of the LDEF-69 Months in Space First Post-Retrieval Symposium, Kissimmee, Florida, June 2-8, 1991, NASA CP-3134 Part 1, pp 569-579.
102	Shipman J., Williamson J., "AIAA Survivability Technical Committee Draft", Aerospace America, December 1997.
103	Cour-Palais B.G. et al, Meteroid Environment Model-1969 (Near Earth to Lunar Surface), NASA SP-8013, 1969.
104	Kessler D.J., Reynolds R.C., Anz-Meador P.D., Orbital Debris Environment for Spacecraft Designed to Operate in Low Earth Orbit, NASA TM-100471, 1988.
105	See T.H., Mack K.S., Warren J.L., Zolensky M.E., and Zook H.A., "Continued Investigation of LDEF's Structural Frame and Thermal Blankets by the Meteoroid and Debris Special Investigation Group", Proceedings of the LDEF-69 Months in Space Second Post-Retrieval Symposium, San Diego, California, June 1-5, 1992, NASA CP-3194 Part 2, pp 313-324.
106	Mandeville J-C. "Micrometeoroids and Debris on LDEF", Proceedings of the LDEF-69 Months in Space Second Post-Retrieval Symposium, San Diego, California, June 1-5, 1992, NASA CP-3194 Part 2, pp 303-312.
107	Bunch T.E., diBrozolo F.R., Fleming R.H., Harris D.W., Brownlee D., Reilly T.W., "LDEF Impact Craters formed by Carbon-Rich Impactors: A Preliminary Report", Proceedings of the LDEF-69 Months in Space First Post-Retrieval Symposium, Kissimmee, Florida, June 2-8, 1991, NASA CP-3134 Part 1, pp 549-564.
108	Stein B.A., Pippin H.G., "Preliminary Findings of the LDEF Materials Special Investigation Group", Proceedings of the LDEF-69 Months in Space First Post-Retrieval Symposium, Kissimmee, Florida, June 2-8, 1991, NASA CP-3134 Part 2, pp 617-641.
109	Zolensky M.E., Zook H.A., Horz F., Atkinson D.R., Coombs C.R., Watts A.J., Dardano C.B., See T.H., Simon C.G., Kinard W.H., "Interim Report of the Meteoroid and Debris Special Investigation Group" Proceedings of the LDEF-69 Months in Space Second Post-Retrieval Symposium, San Diego, California, June 1-5, 1992, NASA CP-3194 Part 2, pp 277-302.
110	Schwinghamer R.J., Whitaker A., "Shield Design for Protection Against Hypervelocity Particles", NASA Tech Briefs , ISSN 0145-319X/ Dec. 1, 1993, p. 76.
111	Christiansen E.L., "Meteoroid/Debris Shielding", NASA TP-2003-210788, August, 2003.

Tables

Table 1: Atomic Oxygen erosion yields of various materials and polymers

Material	Abbrev.	Trade Names	Predicted Erosion Yield in LEO by Different Correlations Re^{LEO} (Ref. 16) ($x10^{-24}$ cm^3/atom)		Erosion Yield in LEO ($x10^{-24}$ cm^3/atom) and references
			γ' mod-Correlation	1/OI Correlation	
Acrylonitrile butadiene styrene	ABS	Cycolac; Lustran	2.3	3.1	
Carbon					0.9-1.7 (Ref. 14)
Carbon (highly oriented pyrolytic graphite)	HOPG	Graphite	1.0	1.3	1.04-1.2 (Ref. 15); 1.2-1.7(Ref. 16); 1.2 (Ref. 14)
Carbon (pyrolytic polycrystalline)	PG	Graphite			0.61-1.2 (Ref. 15); 1.2 (Ref. 14)
Carbon (single crystal natural Class IIA diamond)		Diamond			0.0000 ± 0.000023 (Ref. 15); 0.021 (Ref. 14)
Cellulose acetate	CA	Cellidor; Tenite Acetate	6.8	3.2 (5.2)	
Cellulose nitrate	CN	Celluloid; Xylonite	13.1		
Crystalline polyvinylfluoride w/white pigment	PVF	White Tedlar	3.4	3.0	0.29 (Ref. 15); 3.2 (Ref. 16)
Diallyl diglycol and triallyl cyanurate	ADC	CR-39	6.1	4.6	6.1 (Ref. 16)
Epoxide or epoxy	EP	Epoxy resin	2.9	2.3	2.7 (Ref. 16) Epoxy Resin 5208; 1.7 (Ref. 14)
Ethylene vinyl acetate copolymer	EVAC	Elvax	3.9	3.5	
Ethylene vinyl alcohol copolymer	EVAL (EVOH)	Eval	3.5	3.0	
Ethylene/propylene/diene	EPTR (EPDM)	Nordel; Keltan	2.9	3.0	
Fluorinated ethylene propylene	FEP	Teflon® FEP	0.0	n/a	0.337± 0.005* (Ref. 15); 0.35 (Ref. 15); 0.03-0.05(Ref. 16); 0.037 (Ref. 15); 0.0-<0.05 (Ref. 14)
Halar ethylene-chlorotrifluoroethylene	ECTFE	Halar	2.0	n/a	2.0-2.1(Ref. 15); 1.9(Ref. 16)
Melamine formaldehyde resin	MF	Melmex; Melopas	3.4		
Phenol formaldehyde	PF	Bakelite;	2.3	2.5	

resin		Plenco; Durex			
Poly-(p-phenylene terephthalamide)	PPD-T (PPTA)	Kevlar 29	2.5	2.9	1.5 ± 0.5 Kevlar 29 (Ref. 15); 2.1-4.1 Kevlar 29 (Ref. 16); 4.0 ± 0.5 Kevlar 49 (Ref. 15); 2.1-4.1 Kevlar 49 (Ref. 16)
Polyacrylonitrile	PAN	Acrilan; Barex; Orlon	2.5	4.5	
Polyamide 6 or nylon 6	PA 6	Caprolan; Akulon K; Ultramid	3.7	3.6	2.8 ± 0.2 (Ref. 15); 4.2 (Ref. 16)
Polyamide 66 or nylon 66	PA 66	Maranyl; Zytel; Durethane	3.7	3.6	2.8 ± 0.2 (Ref. 15)
Polybenzimidazole	PBI	Celazole	1.9	1.8	1.5 (Ref. 16); 1.5 (Ref. 14)
Polycarbonate	PC	Lexan; Makrolon	2.9	3.2	2.9 (Ref. 16); 6.0 (Ref. 14)
Polychlorotrifluoroethylene	PCTFE	Kel-F; Aclar	1.0	n/a	1.97 ± 0.12* (Ref. 15); 0.9 (Ref. 16)
Polyetheretherkeytone	PEEK	Victrex PEEK; Hostatec	2.3	2.1	3.7 ± 1.0 (Ref. 15); 2.3 (Ref. 15); 3.2-4.5 (Ref. 16)
Polyethylene	PE	Alathon; Lupolen; Hostalen	3.0	4.2	3.97 ± 0.23 (Ref. 15); 3.2-4.5 (Ref. 16); 3.3 (Ref. 14); 3.7 (Ref. 14)
Polyethylene oxide	PEO	Alkox; Polyox	7.1	5.8	
Polyethylene terephthalate	PET	Mylar; Tenite	3.5	3.1	3.4-3.6 Mylar A (Ref. 15); 3.4-3.7 Mylar A (Ref. 14); 3.0 Mylar D (Ref. 15); 2.9-3.0 Mylar D (Ref. 14); 3.4-3.9 (Ref. 16); 1.5-3.9 (Ref. 14)
Polyimide (PMDA)	PI	Kapton® HN	2.9	2.0	3.0 (Ref. 16); 3.0 (Ref. 14)
Polyimide (PMDA)	PI	Kapton® H	2.9	2.0	3.0 (Ref. 15); 2.89 ± 0.6 (Ref. 15); 3.0 (Ref. 16); 3.0 (Ref. 14); 1.5-3.1 (Ref. 14)
Polyimide (PMDA)	PI	Black Kapton			1.4-2.2 (Ref. 14)
Polymethyl methacrylate	PMMA	Plexiglas; Lucite	5.1	4.5	6.3 ± 0.3 (Ref. 15); 3.9-4.8 (Ref. 16); 3.1 (Ref. 14)

Polyoxymethylene; acetal; polyformaldehyde	POM	Delrin; Celcon; Acetal	8.0-12.0	5.0	
Polyphenylene	PPH		1.8		
Polyphenylene isophthalate	PPPA	Nomex	2.5	2.9	
Polypropylene	PP	Profax; Propathene	2.9	4.1	4.4 (Ref. 15)
Polystyrene	PS	Lustrex; Polystyrol; Styron	2.1	6.0	4.17 ± 0.17 (Ref. 15); 1.8 (Ref. 16)
Polysulphone (Polysulfone)	PSU	Udel; Ultrason/S	2.5	2.4-3.0	2.3 (Ref. 15); 2.1 (Ref16); 2.4 (Ref. 14)
Polytetrafluoroethylene	PTFE	Fluon; Teflon; Halon	0.0	n/a	0.20 (Ref. 15); 0.37 ± 0.06 (Ref. 15); 0.03-0.05 (Ref. 16); 0.0-0.2 (Ref. 14)
Polyvinyl acetate	PVA	Elvacet	6.2		
Polyvinyl alcohol	PVA(L)	Elvanol	7.1	4.1	
Polyvinyl fluoride	PVF	Tedlar			3.8 clear (Ref. 15); 1.3-3.2 clear (Ref. 14); 0.05-0.6 white (Ref. 14)
Polyvinylidene chloride copolymers	PVDC	Saran	5.1	n/a	
Polyvinylidene fluoride	PVDF	Kynar	1.1	n/a	0.9-1.1 (Ref. 16); 0.6 (Ref. 14)
Polyxylylene	PX	Parilene; Parylene	2.1		
Pyrone	PR	Pyrone	2.4		2.3 (Ref. 16); 2.5 (Ref. 14)
Tetrafluoroethylene-ethylene copolymer	ETFE	Tefzel ZM	1.1	n/a	1.2 (Ref. 16)
Urea formaldehyde	UF	Beetle; Avisco	5.1	3.0	

* Corrected for LDEF ram fluence of 9.09×10^{21} atoms/cm^2

Table 2: Air Mass Zero Integrated Solar Irradiance (Ref. 49)

Wavelength Range	Integrated solar irradiance in wavelength range (W/m^2)	Percent of Solar Constant within wavelength range
$\lambda \leq 1000$ μm	1366.1	100
$\lambda \leq 400$ nm	106.6	7.8
$\lambda \leq 200$ nm	0.10	0.007
$\lambda \leq 120.5$ nm	3.12×10^{-4}	2.28×10^{-5}

Table 3: Effect of gamma radiation dose on some common spacecraft polymers (Ref. 80)

	Gamma Radiation Dose (rad)	
Material	Mild to Moderate Damage	Moderate to Severe Damage
Teflon® fluorinated ethylene propylene (FEP)	1E6-8E6	8E6-2E7
Teflon® polytetrafluoroethylene (PTFE)	2E4-1E5	1E5-2E6
Kapton®, polyimide	1E8-1E10	1E10-1E11
Mylar, polyethylene terephthalate (PET)	4E6-1E8	1E8-1E9
Polyethylene	1E7-8E7	8E7-2E8
Polyurethane	1E9-5E9	5E9-2E10
Silicone	1E8-1E9	1E9-5E9
Epoxy	2E8-8E8	8E8-5E9
Nylon, polyamide	3E5-2E6	2E6-2E7
Polyvinyl chloride (PVC)	1E7-7E7	7E7-2E8

Table 4: Solar Absorptance of Original and Reformulated White Paints Before and After Exposure to 2600 Equivalent Sun Hours UV and 3×10^{16} electrons/m^2 at 40 keV energy (calculated from original data in Ref. 88)

White Paint Type	Number of Samples	Avg. Solar Absorptance (pristine)	Avg. Solar Absorptance (post-test)	Avg. Solar Absorptance Increase
Z-93	6	0.118 ± 0.014	0.155 ± 0.013	0.037
Z-93P	6	0.109 ± 0.001	0.152 ± 0.019	0.043
S13GLO-1	6	0.166 ± 0.010	0.287 ± 0.014	0.121
S13GPLO-1	7	0.150 ± 0.009	0.377 ± 0.087	0.227
YB-71	7	0.103 ± 0.021	0.238 ± 0.054	0.135
YB-71P	9	0.091 ± 0.013	0.345 ± 0.037	0.254

Table 5. HST Thermal Control Candidate Replacement Materials

Material	Sample Id.	Candidate Material
1	B1.1 and M2.1	10 mil FEP/Ag/Inconel/adhesive/Nomex® (polyphenylene isophthalate) scrim
2	B1.2 and M2.2	5 mil FEP/Ag/Inconel/adhesive/fiberglass scrim/adhesive/2 mil Kapton®
3	B1.3 and M2.3	10 mil FEP/Al/adhesive/Nomex® scrim
4	B1.4 and M2.4	5 mil FEP/A1/adhesive/fiberglass scrim/adhesive/2 mil Kapton®
5	B1.5 and M2.5	5 mil FEP/Ag/Inconel/adhesive/Nomex® scrim
6	B1.6 and M2.6	5 mil FEP/A1/adhesive/Nomex® scrim
7	B1.7 and M2.7	OCLI multi-layer oxide UV blocker/2 mil white Tedlar®
8	B1.8 and M2.8	5 mil FEP/Al (current HST material)
9	B1.9 and M2.9	$SiO_2/Al_2O_3/Ag/Al_2O_3$/4 mil stainless steel
10	B1.0 and M2.0	Proprietary Teflon® FEP/AZ93 White Paint/Kapton®

Figure Captions

Figure 1. Density of atmospheric species as a function of altitude.

Figure 2. Atomic oxygen flux versus altitude for solar minimum, nominal (standard atmosphere), and solar maximum conditions.

Figure 3. Atomic oxygen fluence per year during a solar cycle.

Figure 4. Atomic oxygen arrival flux relative to the ram direction for a 400 km orbit at 28.5° inclination and 1000 K thermosphere.

Figure 5. Polar plot of relative atomic oxygen flux as a function of the angle between the ram direction and the normal of the arrival surface for a LEO spacecraft in a 400 km orbit at 28.5° inclination and 1000 K thermosphere.

Figure 6. Energy distribution of atomic oxygen atoms as a function of altitude for a circular orbit at 28.5° inclination and 1000 K thermosphere.

Figure 7. Low Earth orbital glow phenomena.
a. Photograph of space shuttle during daylight.
b. Photograph of space shuttle at night.

Figure 8. Atomic oxygen reaction pathways with polymers.

Figure 9. Surface oxygen content (measured using XPS) for chlorotrifluoroethylene as a function of atomic oxygen exposure level, where exposures were conducted in ground facility RF air plasma.

Figure 10. Photographs comparing unexposed DC 93-500 silicone to the same surface after exposure to an atomic oxygen fluence of 2.3×10^{20} atoms/cm^2 in LEO during shuttle flight STS-46.

Figure 11. Scanning electron microscope photograph of DC 93-500 silicone showing cracking and subsequent branch cracking after atomic oxygen exposure to an effective fluence of $2.6x10^{21}$ atoms/cm^2 in a plasma asher facility.

Figure 12. Scanning electron microscope photographs of LEO atomic oxygen textured polymers. a) Kapton® H polyimide, b) Fluorinated ethylene propylene (FEP) Teflon, c) Chlorotrifluoroethylene

Figure 13. Scanning electron microscope photographs of LEO atomic oxygen exposed Kapton® from LDEF at sites of pinwindow and crack defects in a vacuum deposited aluminum protective coating.

a) Prior to removal of aluminized coating

b) After chemical removal of protective coating

Figure 14. MIR solar array sun facing surface after 10 years in LEO

(a) Photograph showing silica contamination as a diffuse white deposit on the front surface of the solar cells.

(b) Scanning electron microscope photograph of oxidized silicone contamination layer.

Figure 15. Back surface of MIR solar cell after 10 years in LEO with tape peeled areas to show comparison of the "tape peeled cleaned" versus the contaminated optical solar reflector glass.

Figure 16. The air mass zero (AM0) solar spectrum:

(a) the wavelength range up to 2500 nm

(b) the UV portion of the AM0 solar spectrum from 100-400 nm

Figure 17. Transmittance as a function of FEP thickness.

Figure 18. Dose-depth for ionizing radiation in FEP for (a) solar flare x-ray exposure and (b) trapped electron and proton radiation exposure for the Hubble Space Telescope environment.

Figure 19. Backscattered electron micrograph showing thermal cycle induced microcracks in an Al/Cr coated graphite epoxy sample which was located on the leading edge of LDEF.

Figure 20. Sample of 2 mil thick FEP with OCLI oxide coating (total coating thickness in range of 700 to 1400 nm) following electron radiation exposure and thermal cycling. Dark regions indicate areas where coating is missing.

Figure 21. Large cracks in outer layer of solar facing MLI on HST as observed during SM2, after 6.8 years in space.

Figure 22. Charged particle radiation and radiation with sequential thermal cycling effects on (a) ultimate tensile strength and (b) elongation of 5 mil Teflon® FEP with comparison to FEP retrieved from HST during SM1 (3.6 years in space) and during SM2 (6.8 years in space).

Figure 23. Change in the slope of the percent elongation at failure data of pristine, ground laboratory x-ray exposed (areal dose of 33.8 kJ/m2) and HST FEP (retrieved after 9.7 years of space exposure) as function of vacuum heat treatment temperature.

Figure 24. Candidate Hubble Space Telescope MLI (a) samples B1.1 - B1.4 and (b) samples B1.5-B1.8 under tension in the Rapid Thermal Cycling Facility after 1000 thermal cycles.

Figure 25. Micrometeoroid and debris particle diameter versus flux.

Figure 26. Angular dependence of impacts around the LDEF spacecraft.

Figure 27. Scanning electron microscope photographs of impact craters on the LDEF spacecraft

a. Aluminum

b. Fluorinated ethylene propylene (FEP) Teflon

Figure 28. Photograph of impact site on Fluorinated ethylene propylene (FEP) Teflon® that was backed with silver and Z 306 paint.

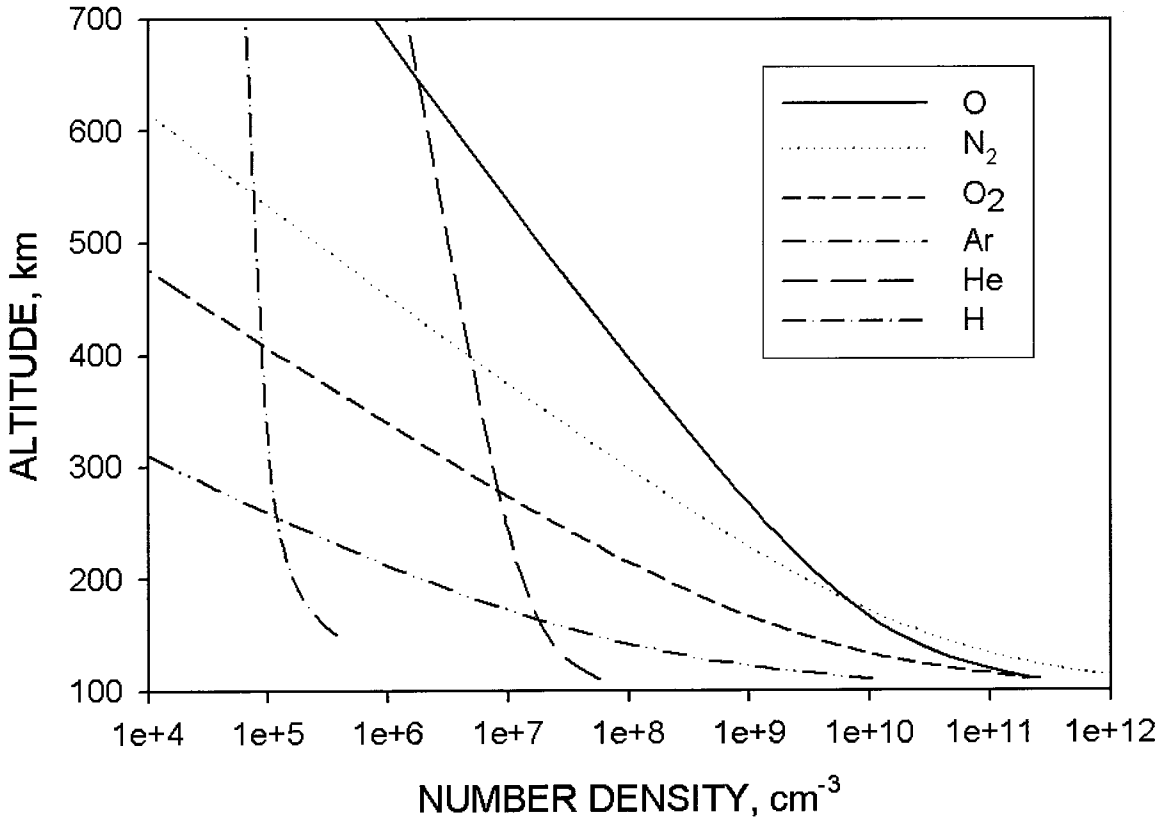
700
600
500
400
300
200
100
ALTITUDE, km
1e+4
1e+5
1e+6
1e+7
1e+8
1e+9
1e+10
1e+11
1e+12
NUMBER DENSITY, cm-3
O
N2
O2
Ar
He
H

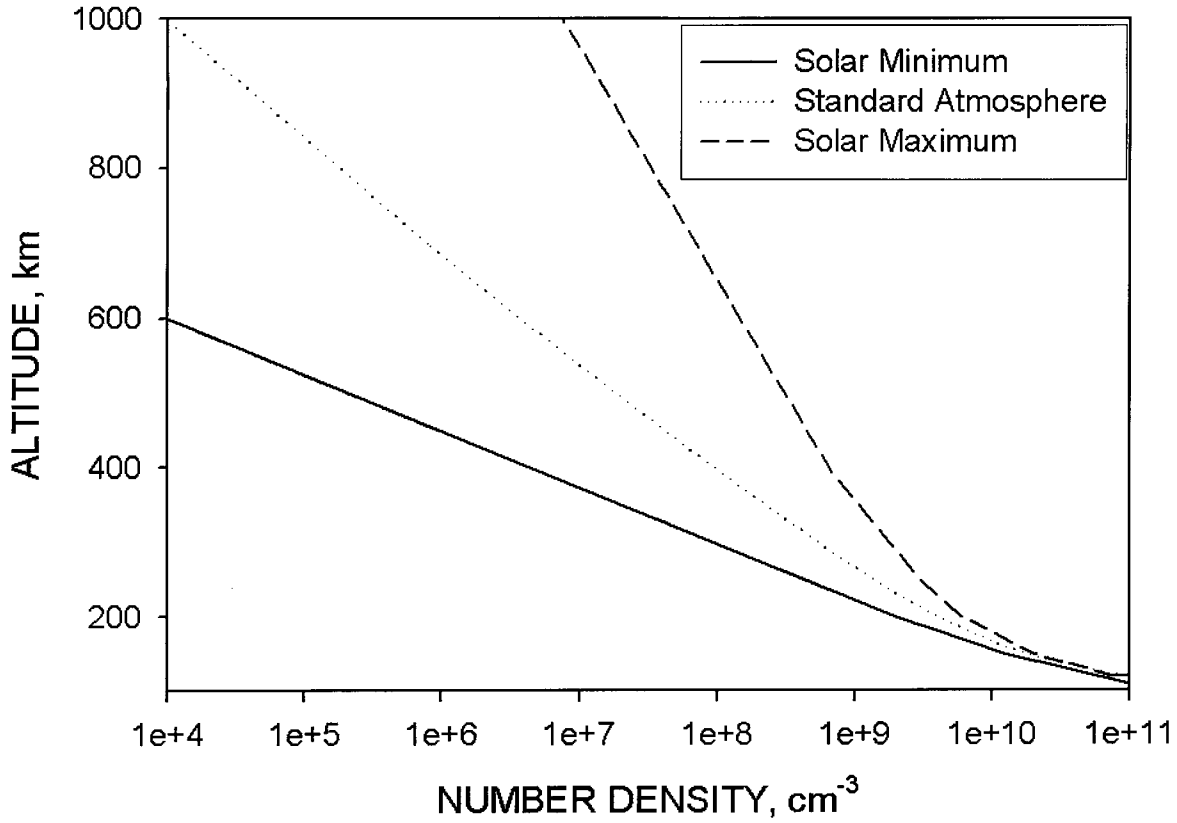
1000
800
600
400
200
ALTITUDE, km
Solar Minimum
Standard Atmosphere
Solar Maximum
1e+4
1e+5
1e+6
1e+7
1e+8
1e+9
1e+10
1e+11
NUMBER DENSITY, cm-3

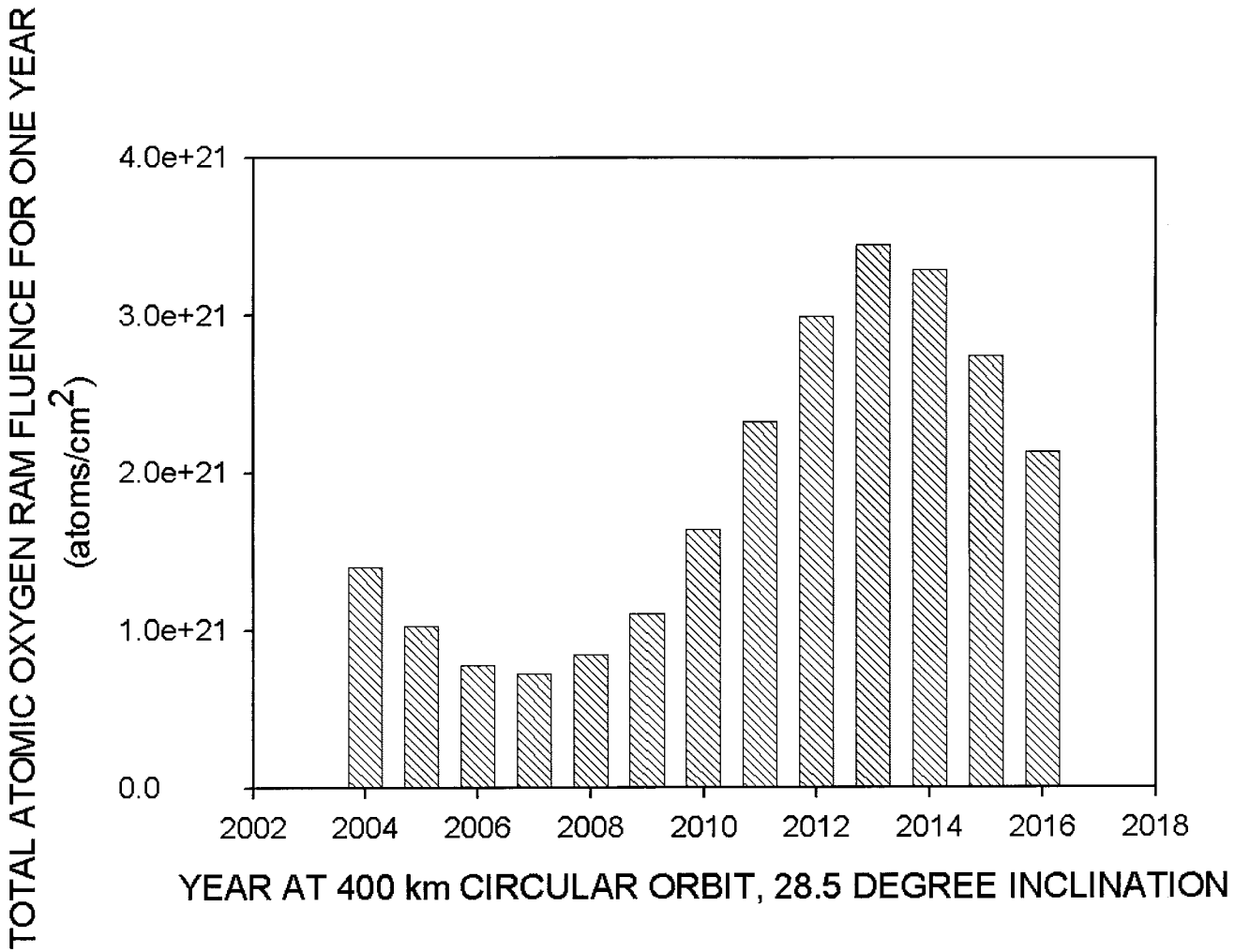
TOTAL ATOMIC OXYGEN RAM FLUENCE FOR ONE YEAR
(atoms/cm2)
4.0e+21
3.0e+21
2.0e+21
1.0e+21
0.0
2002
2004
2006
2008
2010
2012
2014
2016
2018
YEAR AT 400 km CIRCULAR ORBIT, 28.5 DEGREE INCLINATION

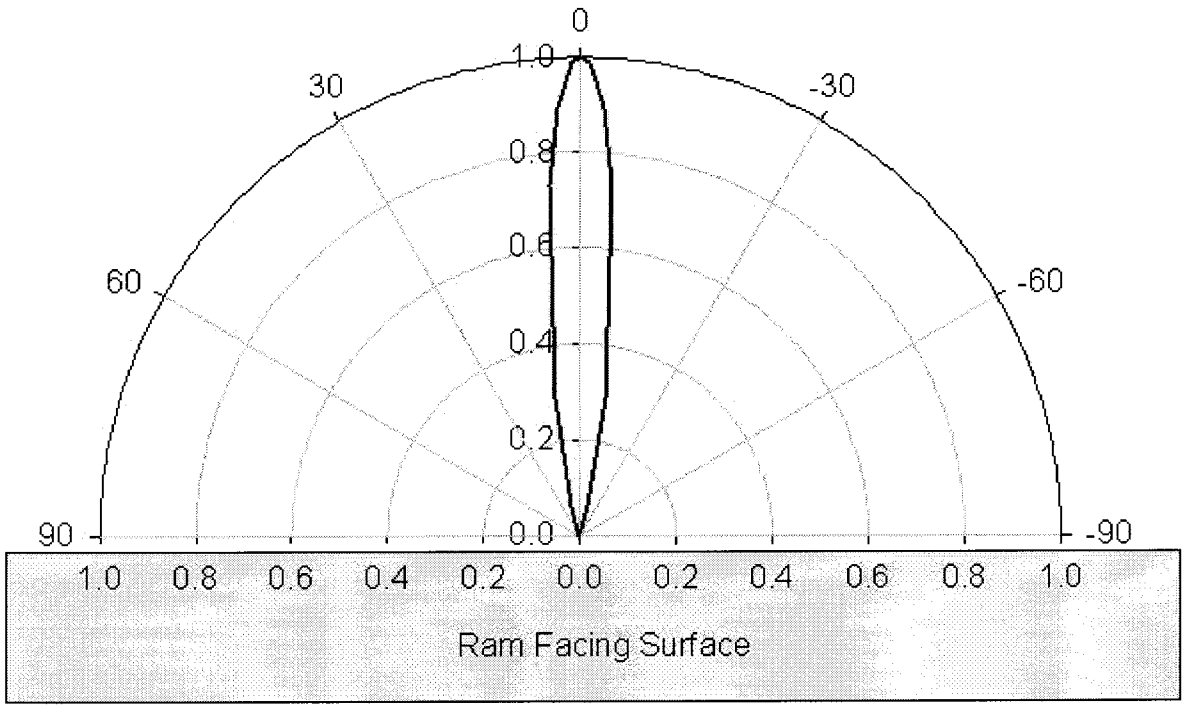
0
1.0
30
-30
0.8
0.6
60
-60
0.4
0.2
90
0.0
-90
1.0 0.8 0.6 0.4 0.2 0.0 0.2 0.4 0.6 0.8 1.0
Ram Facing Surface

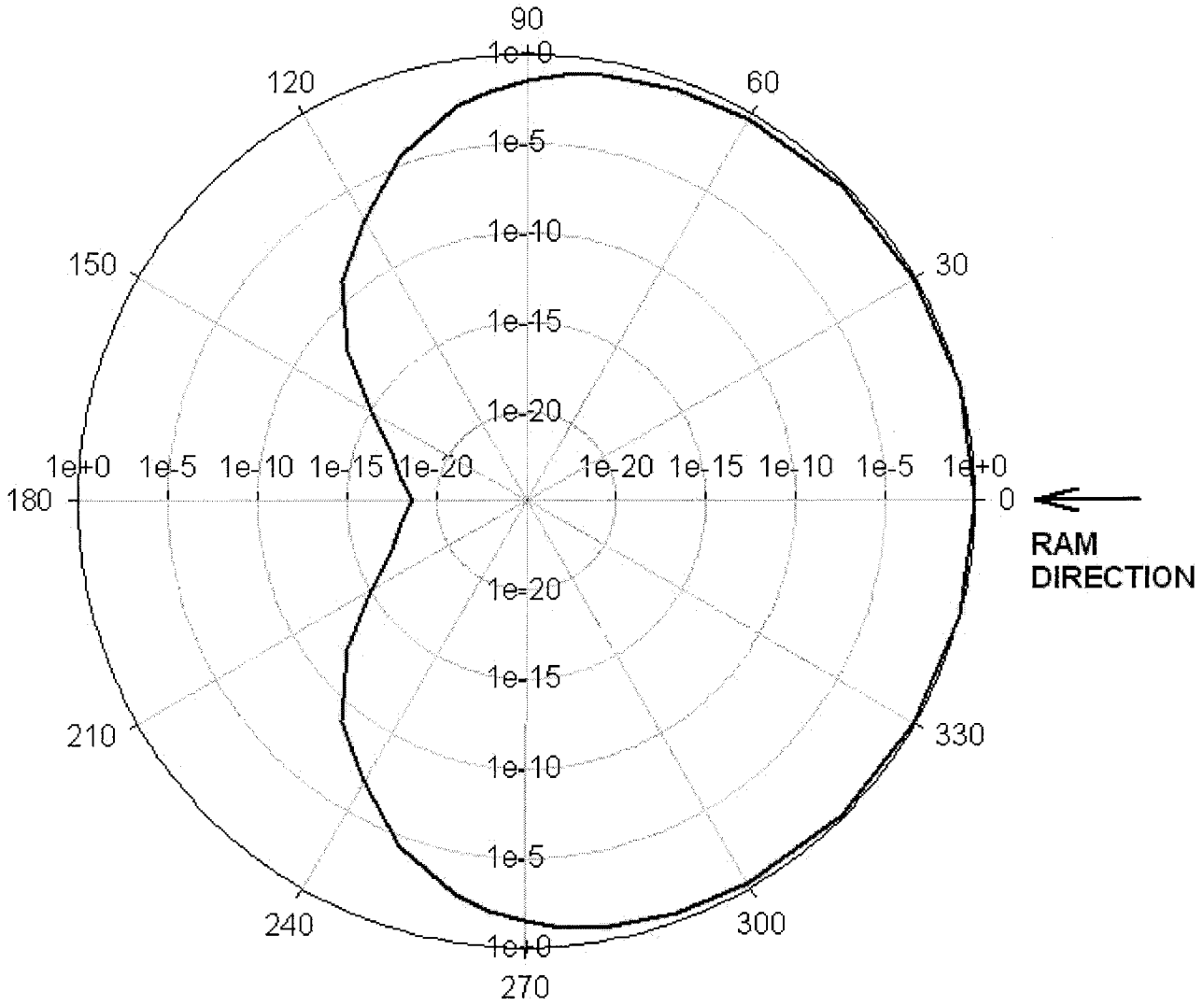
90
1e+0
120
60
1e-5
1e-10
150
30
1e-15
1e-20
1e+0 1e-5 1e-10 1e-15 1e-20
1e-20 1e-15 1e-10 1e-5 1e+0
180
0
RAM
DIRECTION
1e-20
1e-15
210
330
1e-10
1e-5
240
300
1e+0
270

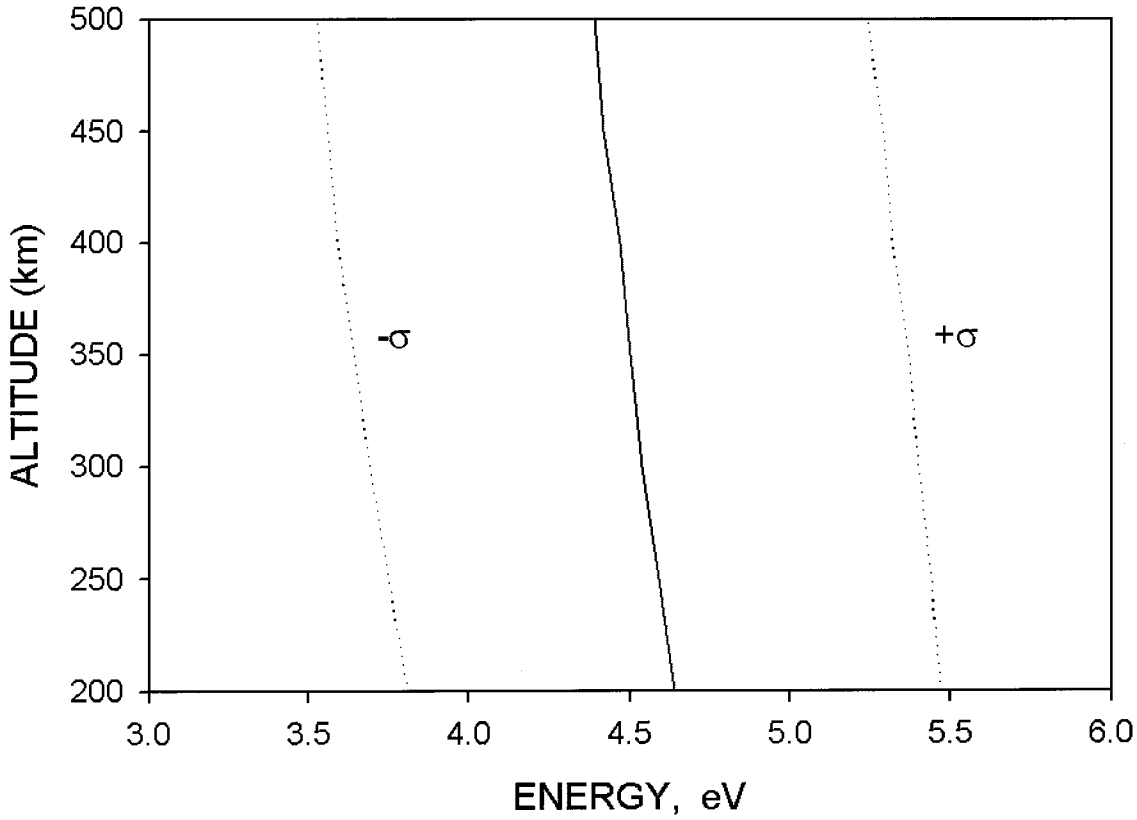
500
450
400
350
300
250
200
ALTITUDE (km)
-σ
+σ
3.0
3.5
4.0
4.5
5.0
5.5
6.0
ENERGY, eV

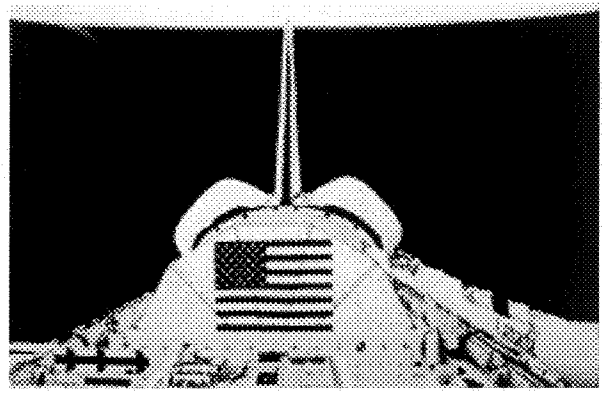

A.

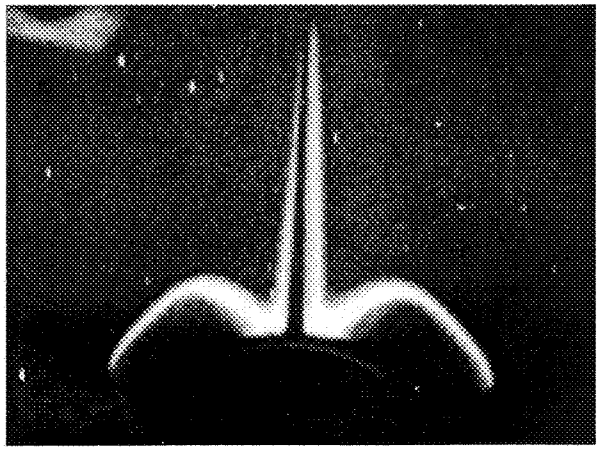

B.

7a and b

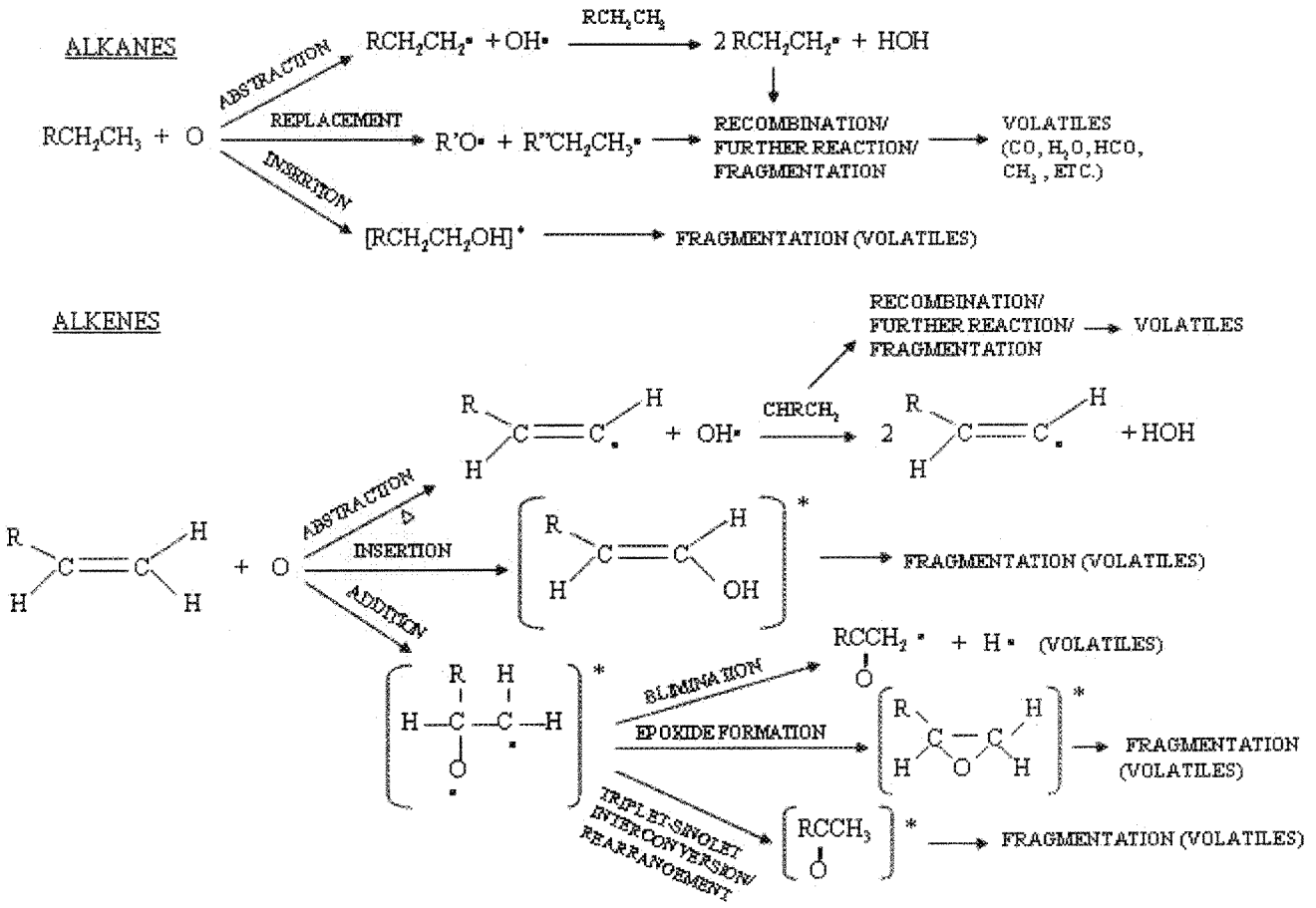
ALKANES
ABSTRACTION
REPLACEMENT
INSERTION
RCH2CH2• +OH•
RCH2CH3
2 RCH2CH2• + HOH
RCH2CH3 + O
R'O• + R"CH2CH3•
RECOMBINATION/
FURTHER REACTION/
FRAGMENTATION
VOLATILES
(CO, H2O, HCO,
CH3, ETC.)
[RCH2CH2OH]•
FRAGMENTATION (VOLATILES)
ALKENES
RECOMBINATION/
FURTHER REACTION/
FRAGMENTATION
VOLATILES
CHRCH2
+ OH•
+HOH
ABSTRACTION
INSERTION
ADDITION
FRAGMENTATION (VOLATILES)
RCCH2 •
+ H •
(VOLATILES)
ELIMINATION
EPOXIDE FORMATION
FRAGMENTATION
(VOLATILES)
TRIPLET-SINGLET
INTERCONVERSION/
REARRANGEMENT
RCCH3
FRAGMENTATION (VOLATILES)

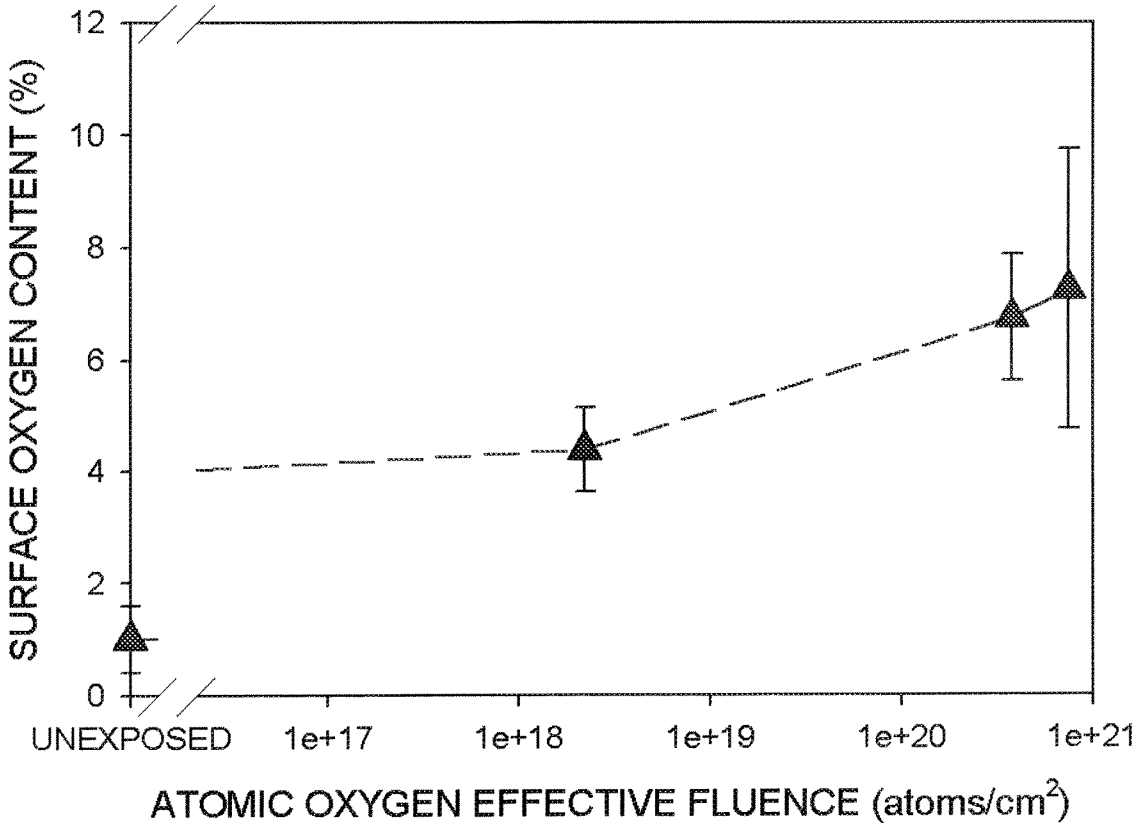
SURFACE OXYGEN CONTENT (%)
12
10
8
6
4
2
0
UNEXPOSED
1e+17
1e+18
1e+19
1e+20
1e+21
ATOMIC OXYGEN EFFECTIVE FLUENCE (atoms/cm2)

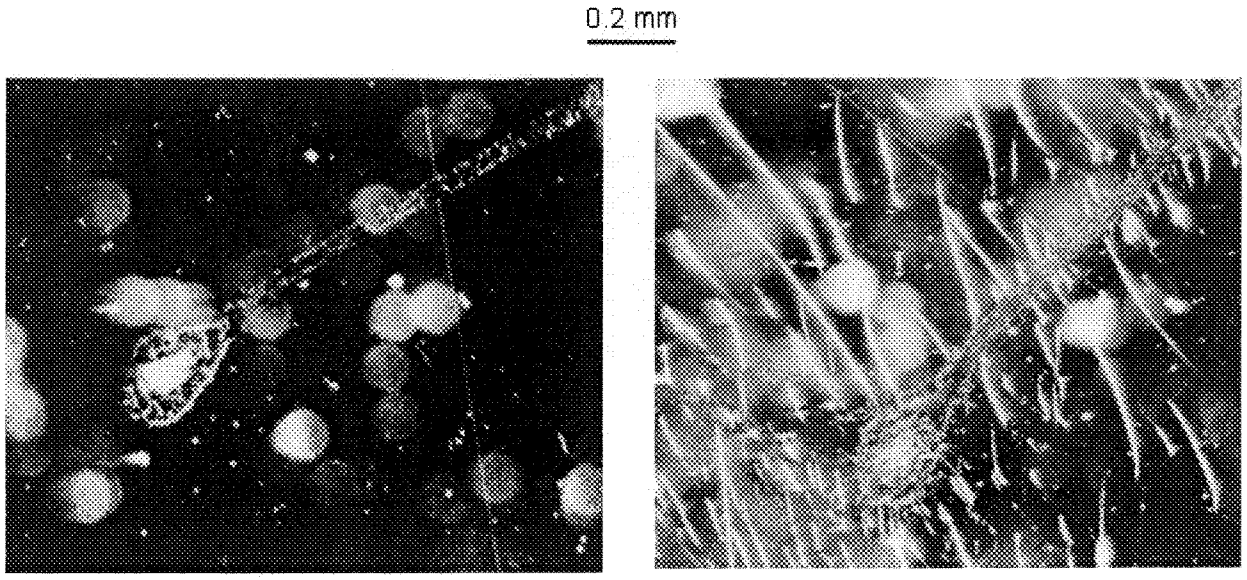

10 a and b

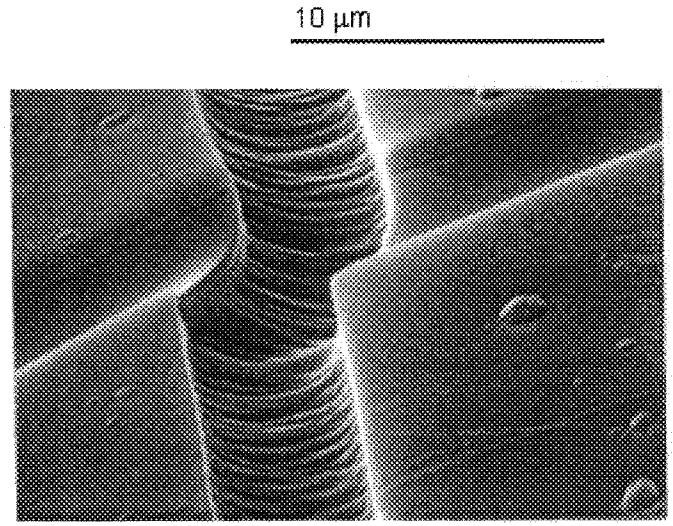
10 µm

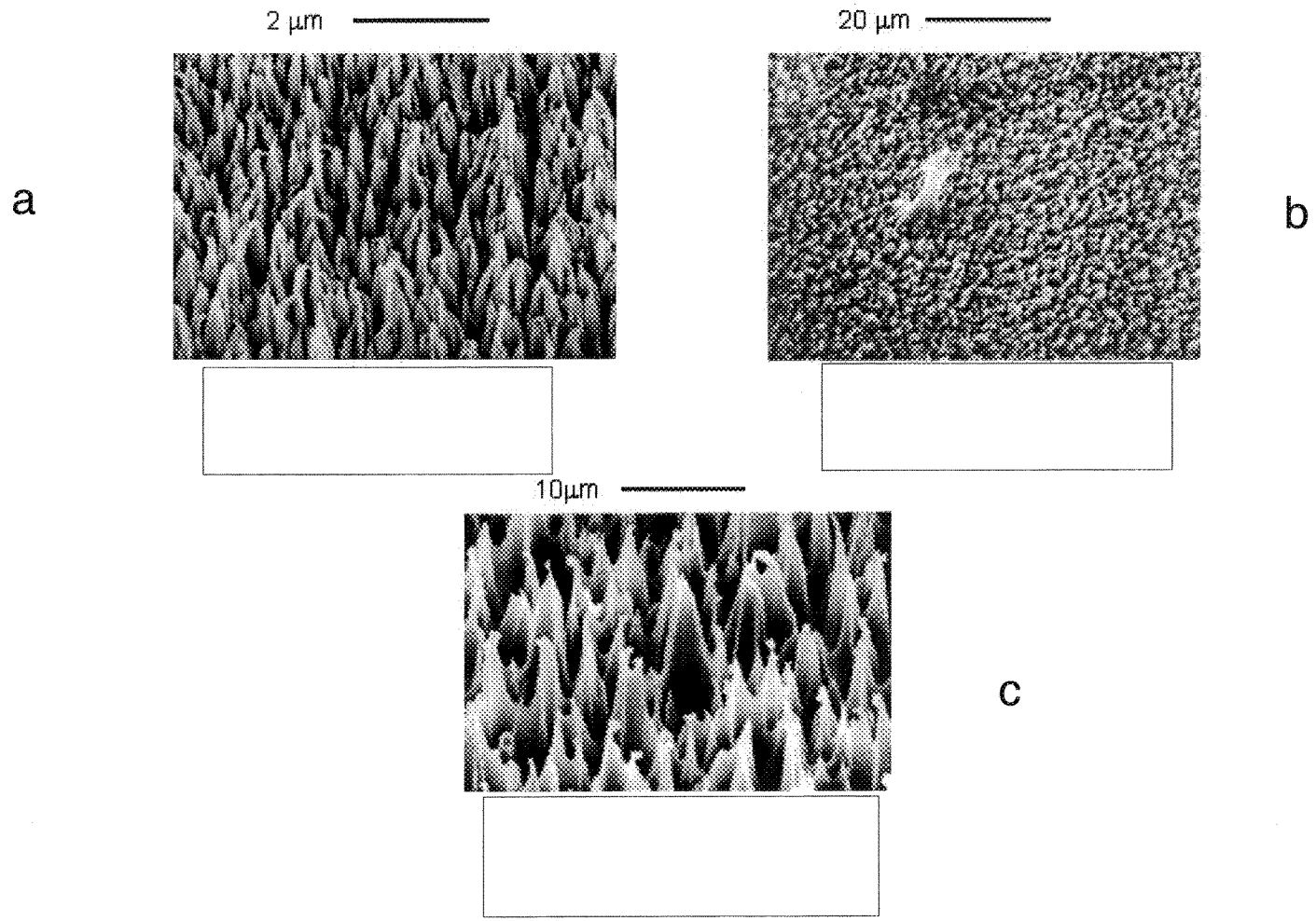

12 a, b and c

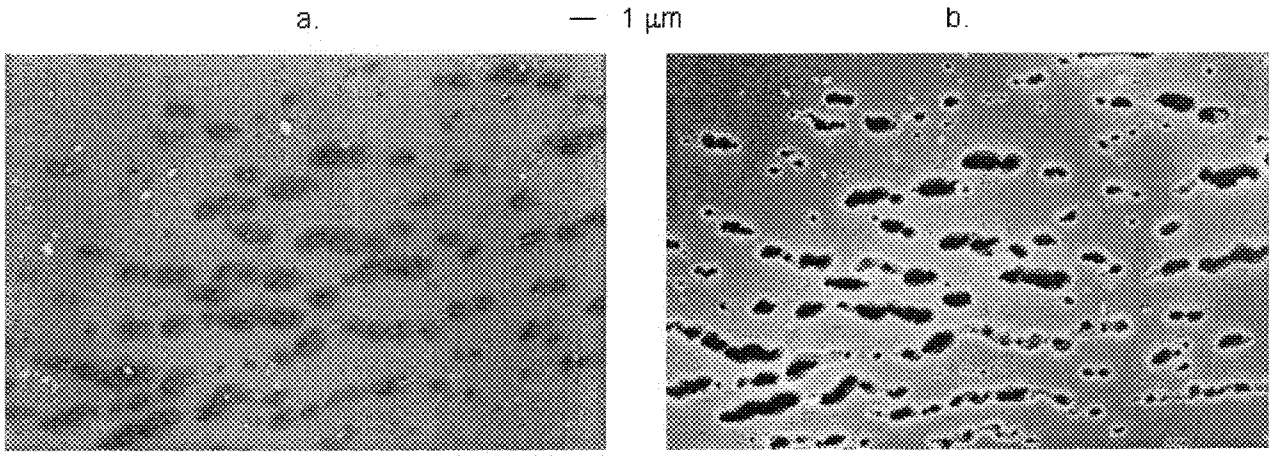

13 a and b

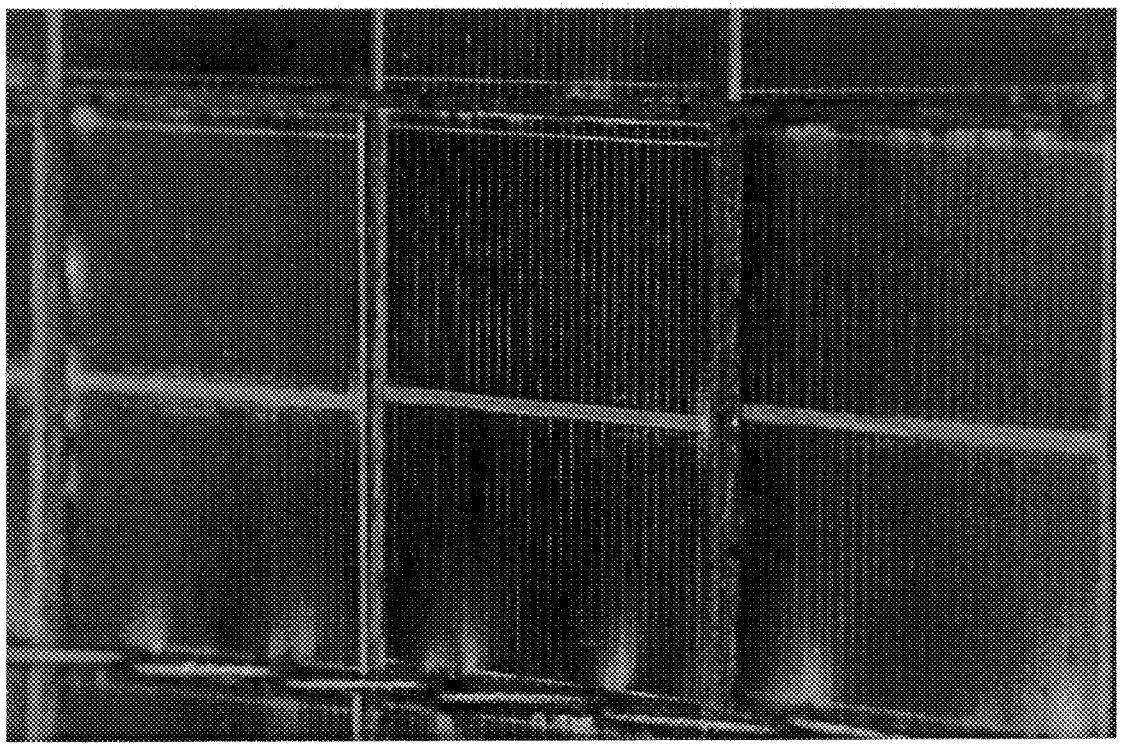

14 a

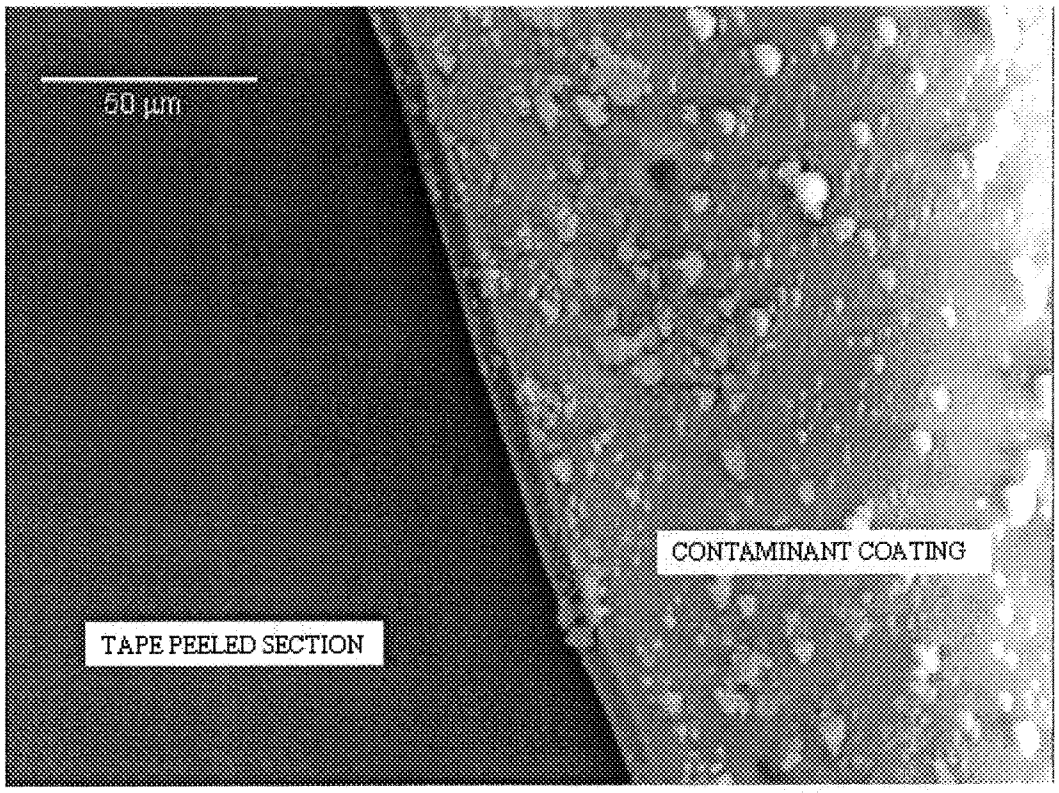

14 b

a

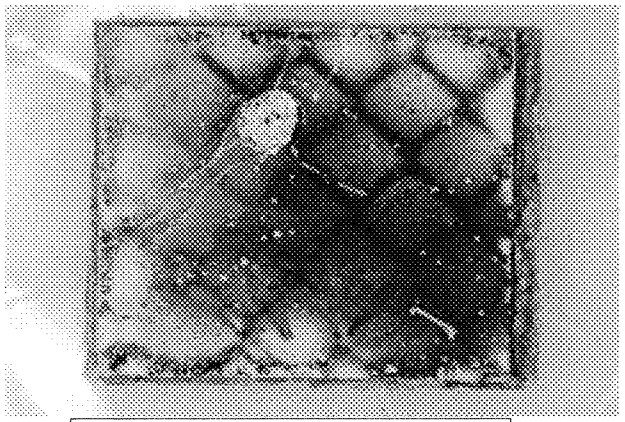

b

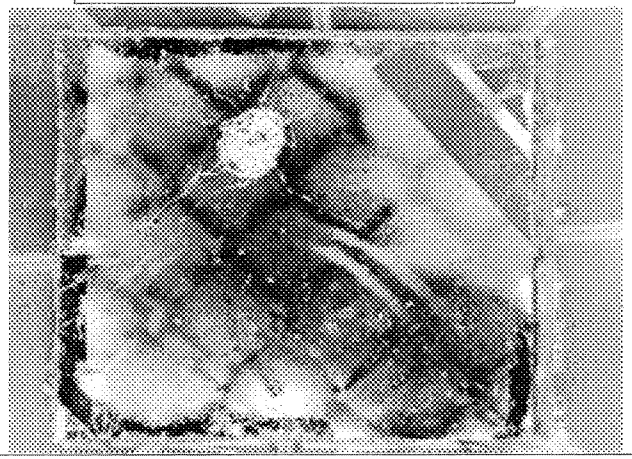

15 a and b

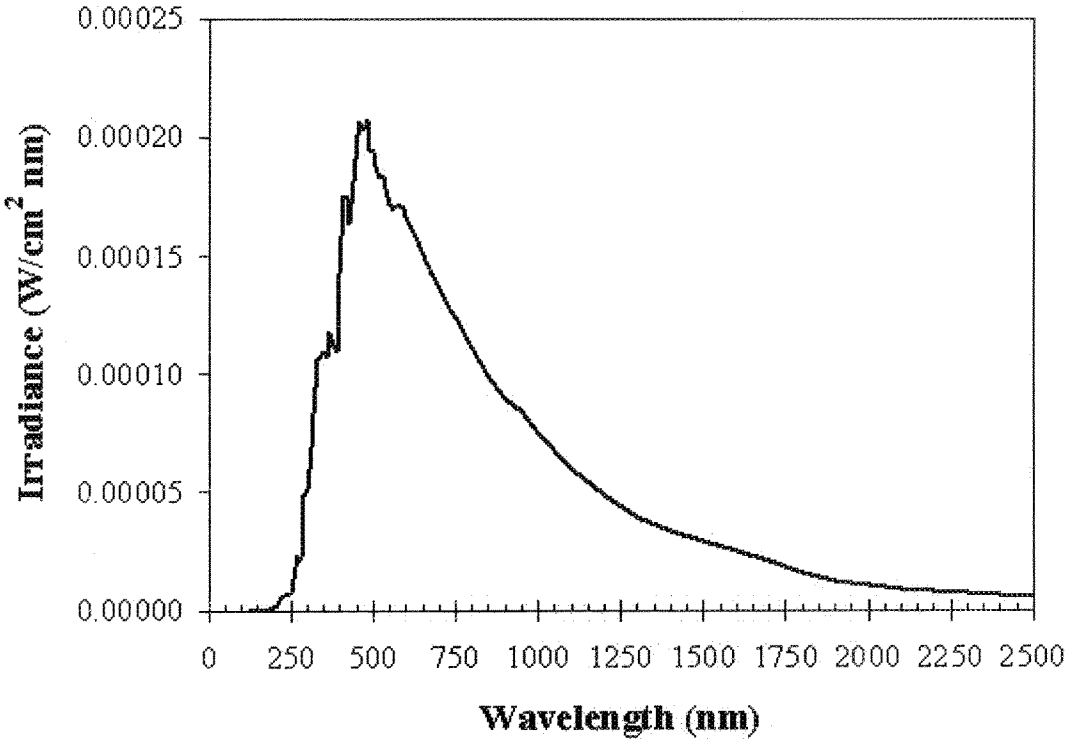
0.00025
0.00020
0.00015
0.00010
0.00005
0.00000
Irradiance (W/cm^2 nm)
0
250
500
750
1000
1250
1500
1750
2000
2250
2500
Wavelength (nm)

16 a

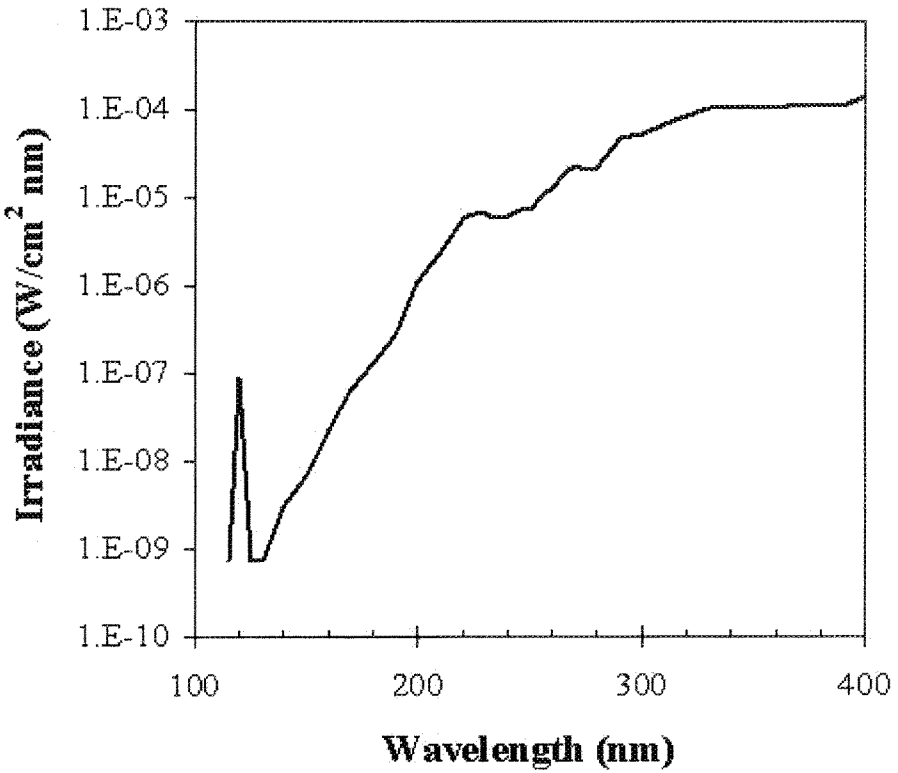
1.E-03
1.E-04
1.E-05
1.E-06
1.E-07
1.E-08
1.E-09
1.E-10
Irradiance (W/cm^2 nm)
100
200
300
400
Wavelength (nm)

16 b

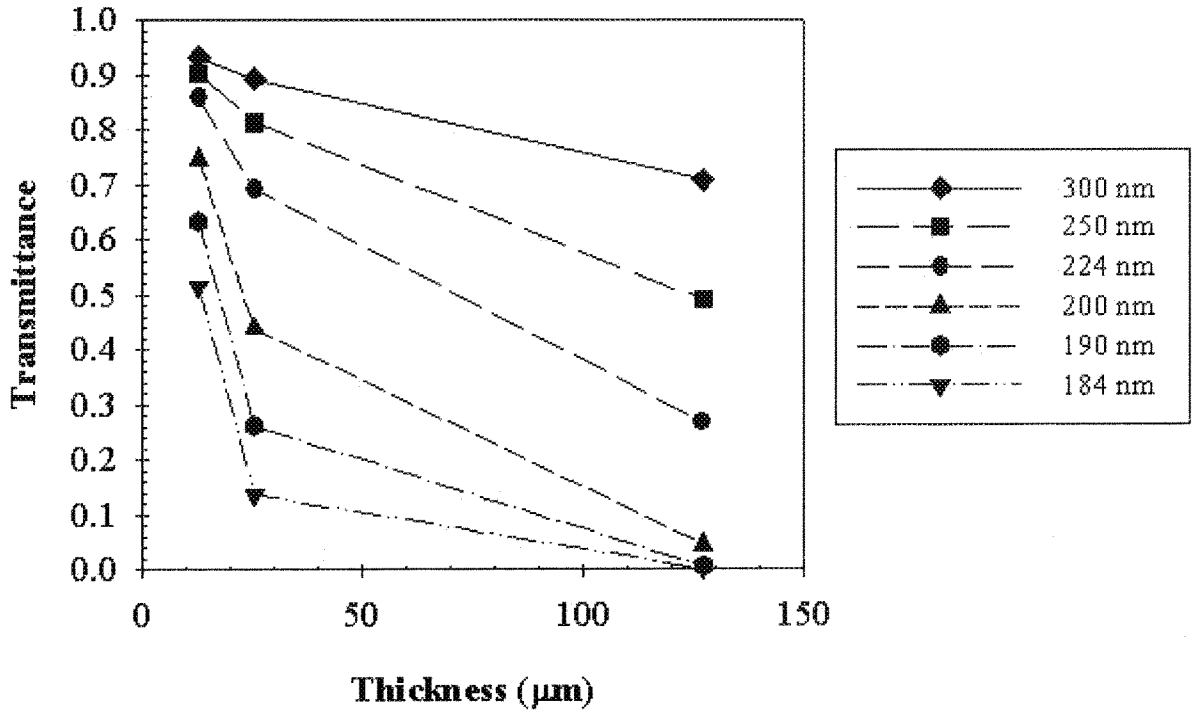
1.0
0.9
0.8
0.7
0.6
0.5
0.4
0.3
0.2
0.1
0.0
Transmittance
0
50
100
150
Thickness (μm)
300 nm
250 nm
224 nm
200 nm
190 nm
184 nm

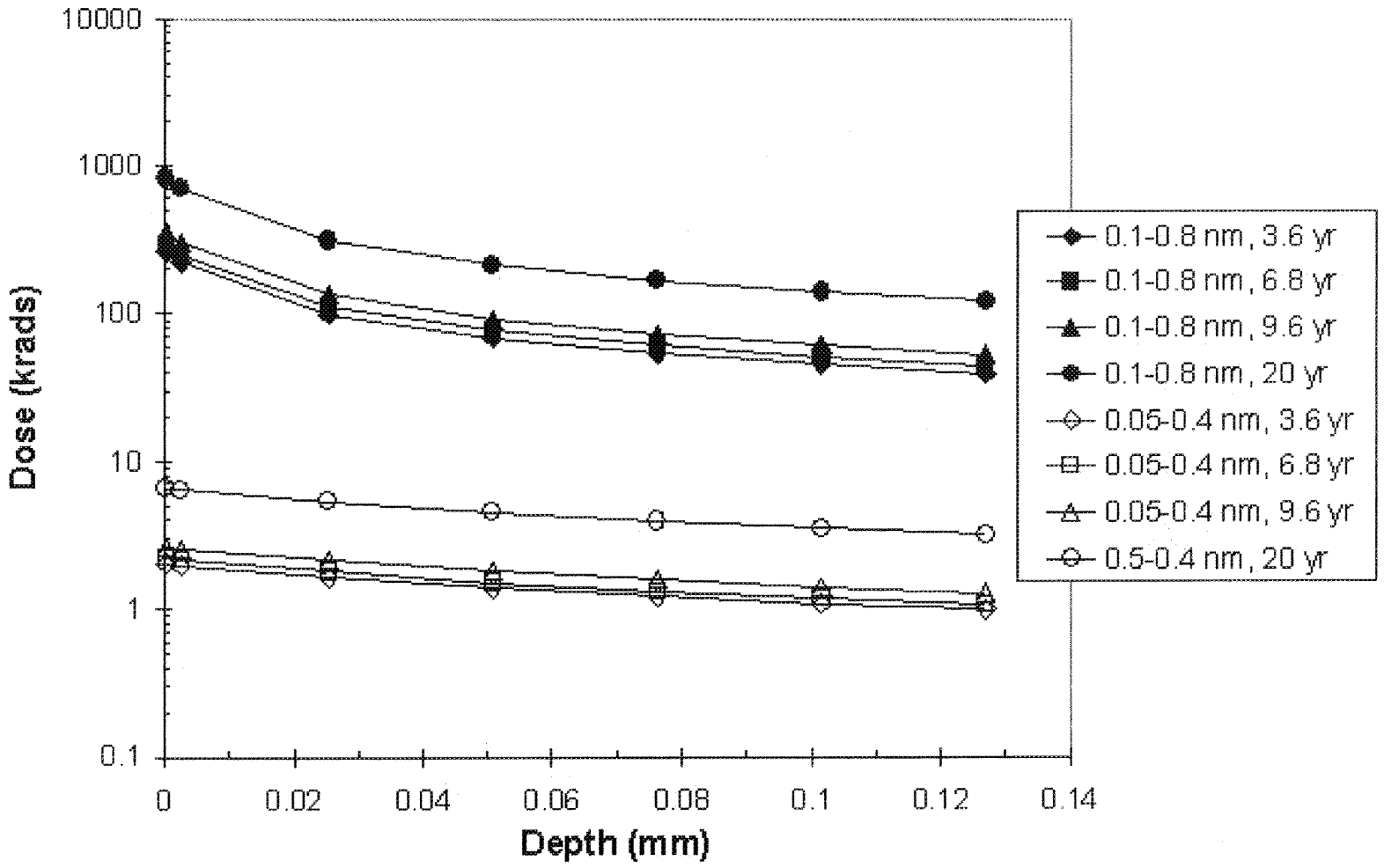
10000
1000
100
10
1
0.1
Dose (krads)
0
0.02
0.04
0.06
0.08
0.1
0.12
0.14
Depth (mm)
0.1-0.8 nm, 3.6 yr
0.1-0.8 nm, 6.8 yr
0.1-0.8 nm, 9.6 yr
0.1-0.8 nm, 20 yr
0.05-0.4 nm, 3.6 yr
0.05-0.4 nm, 6.8 yr
0.05-0.4 nm, 9.6 yr
0.5-0.4 nm, 20 yr

18 a

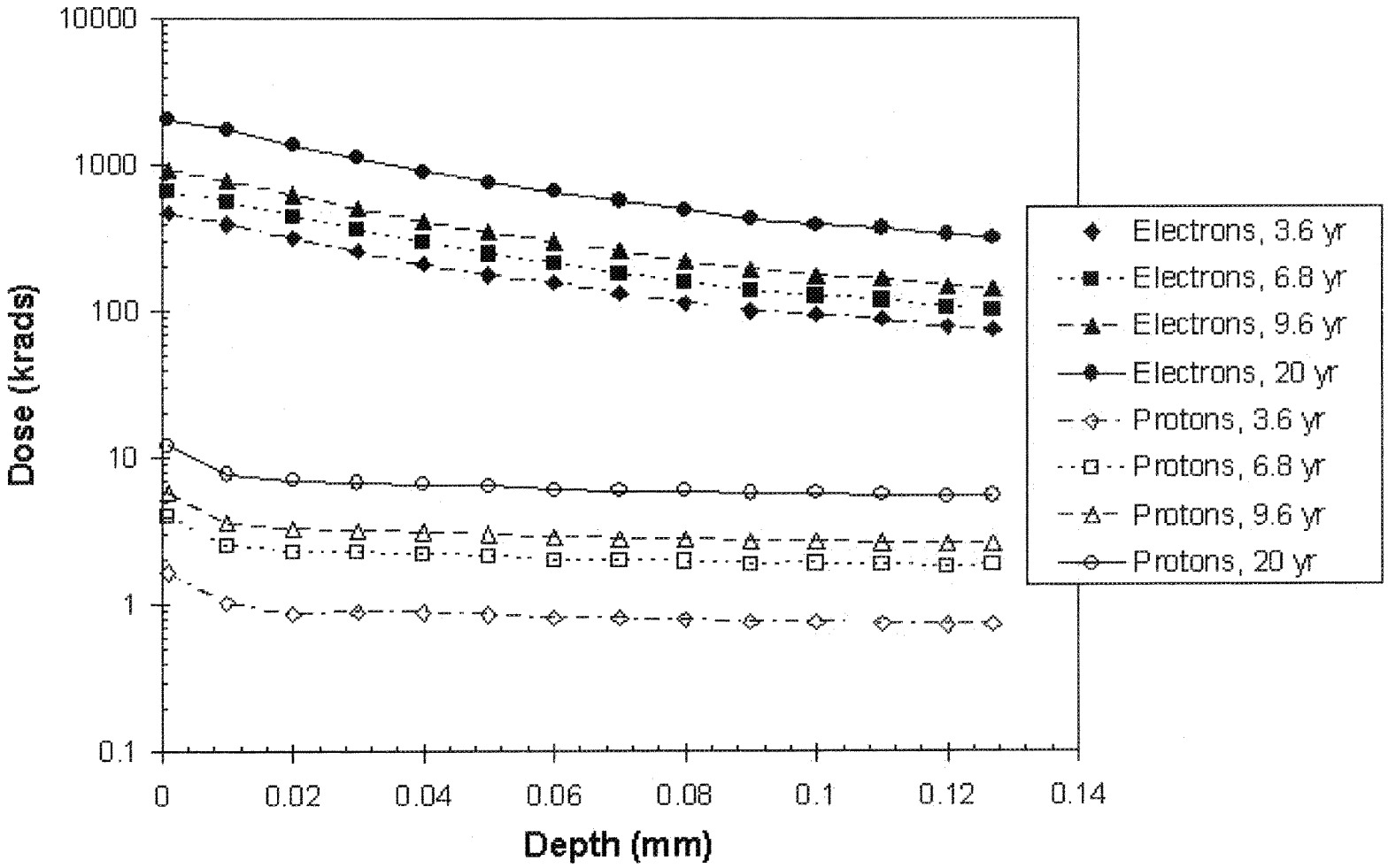
10000
1000
100
10
1
0.1
Dose (krads)
0
0.02
0.04
0.06
0.08
0.1
0.12
0.14
Depth (mm)
Electrons, 3.6 yr
Electrons, 6.8 yr
Electrons, 9.6 yr
Electrons, 20 yr
Protons, 3.6 yr
Protons, 6.8 yr
Protons, 9.6 yr
Protons, 20 yr

18 b

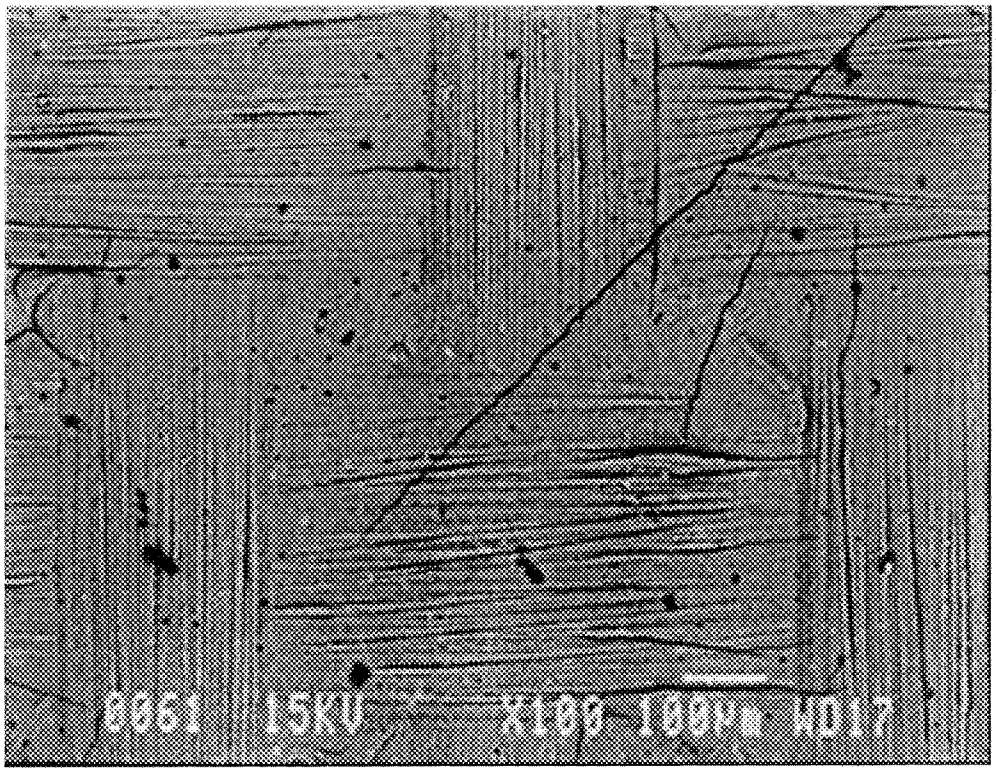
0061 15KV X100 100μm WD17

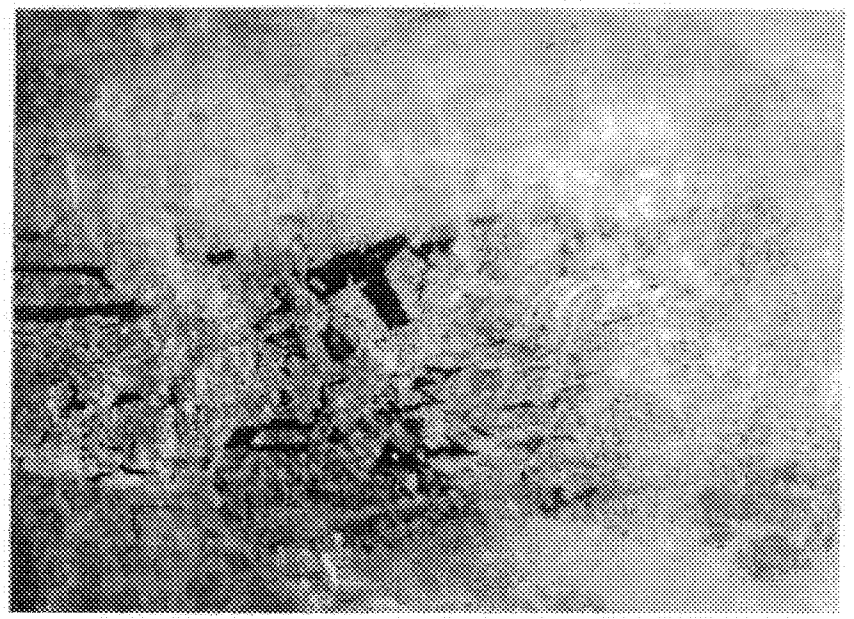

— 0.5 mm

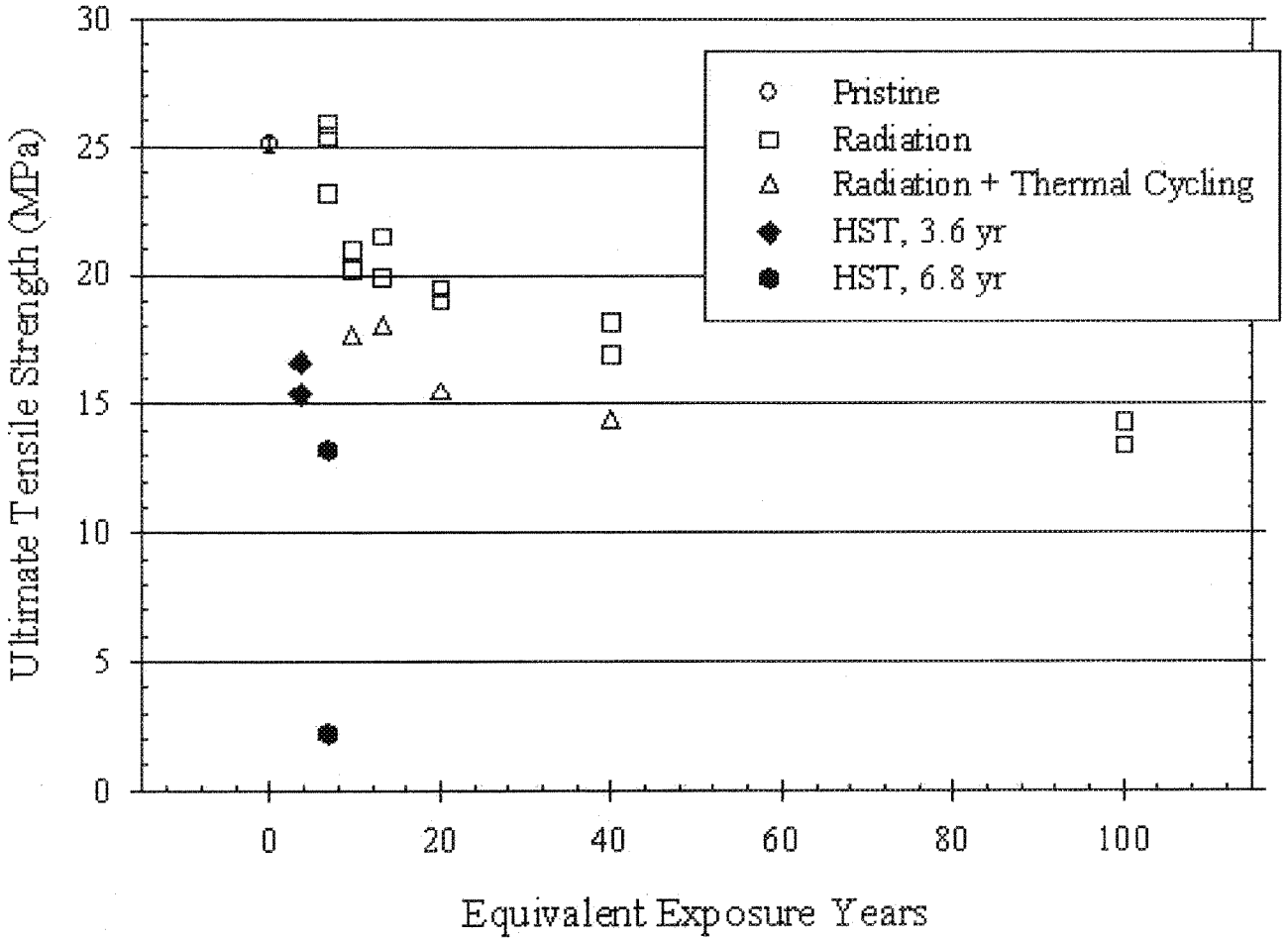
Ultimate Tensile Strength (MPa)
30
25
20
15
10
5
0
0
20
40
60
80
100
Equivalent Exposure Years
Pristine
Radiation
Radiation + Thermal Cycling
HST, 3.6 yr
HST, 6.8 yr

22 a

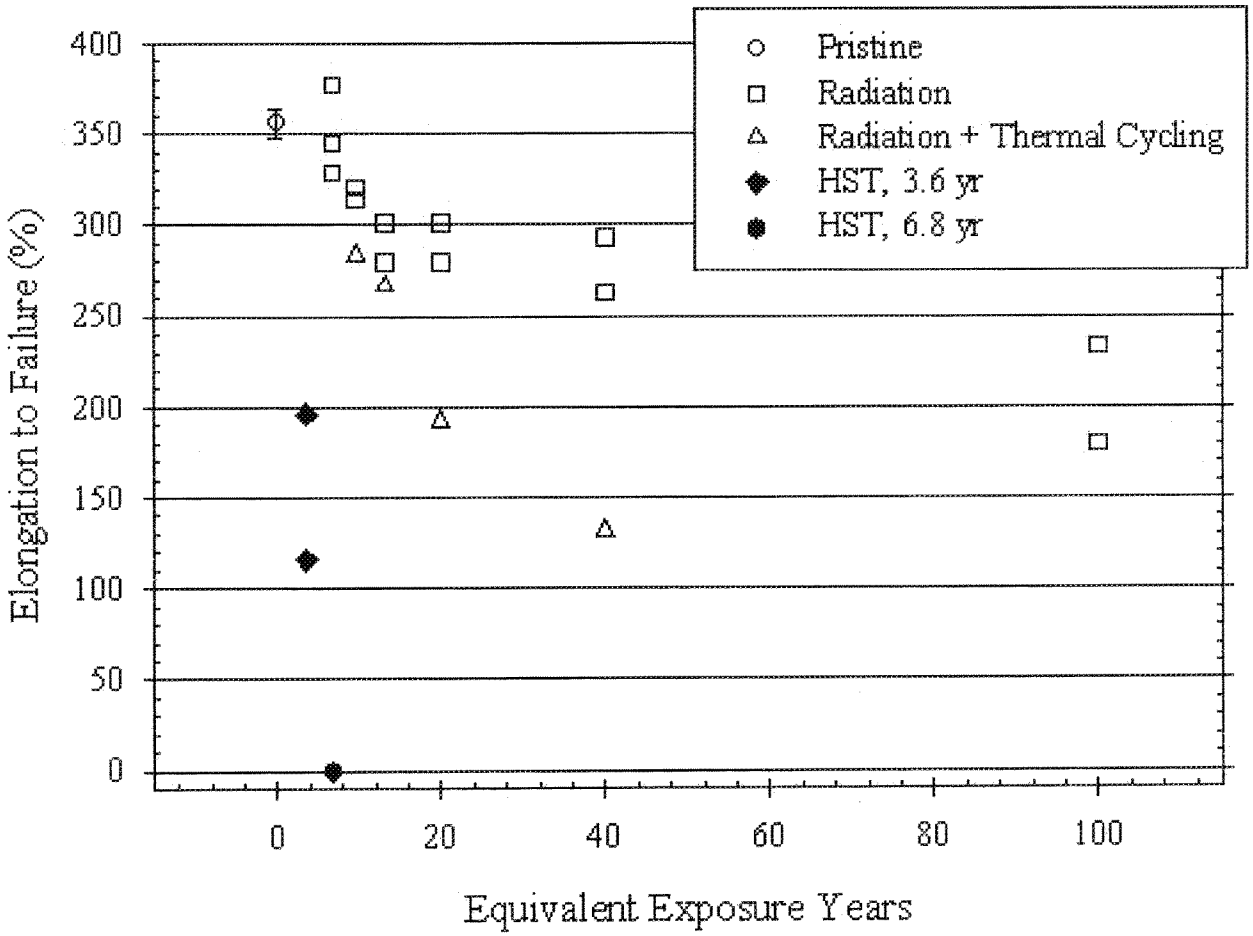
Pristine
Radiation
Radiation + Thermal Cycling
HST, 3.6 yr
HST, 6.8 yr
Elongation to Failure (%)
400
350
300
250
200
150
100
50
0
0
20
40
60
80
100
Equivalent Exposure Years

22 b

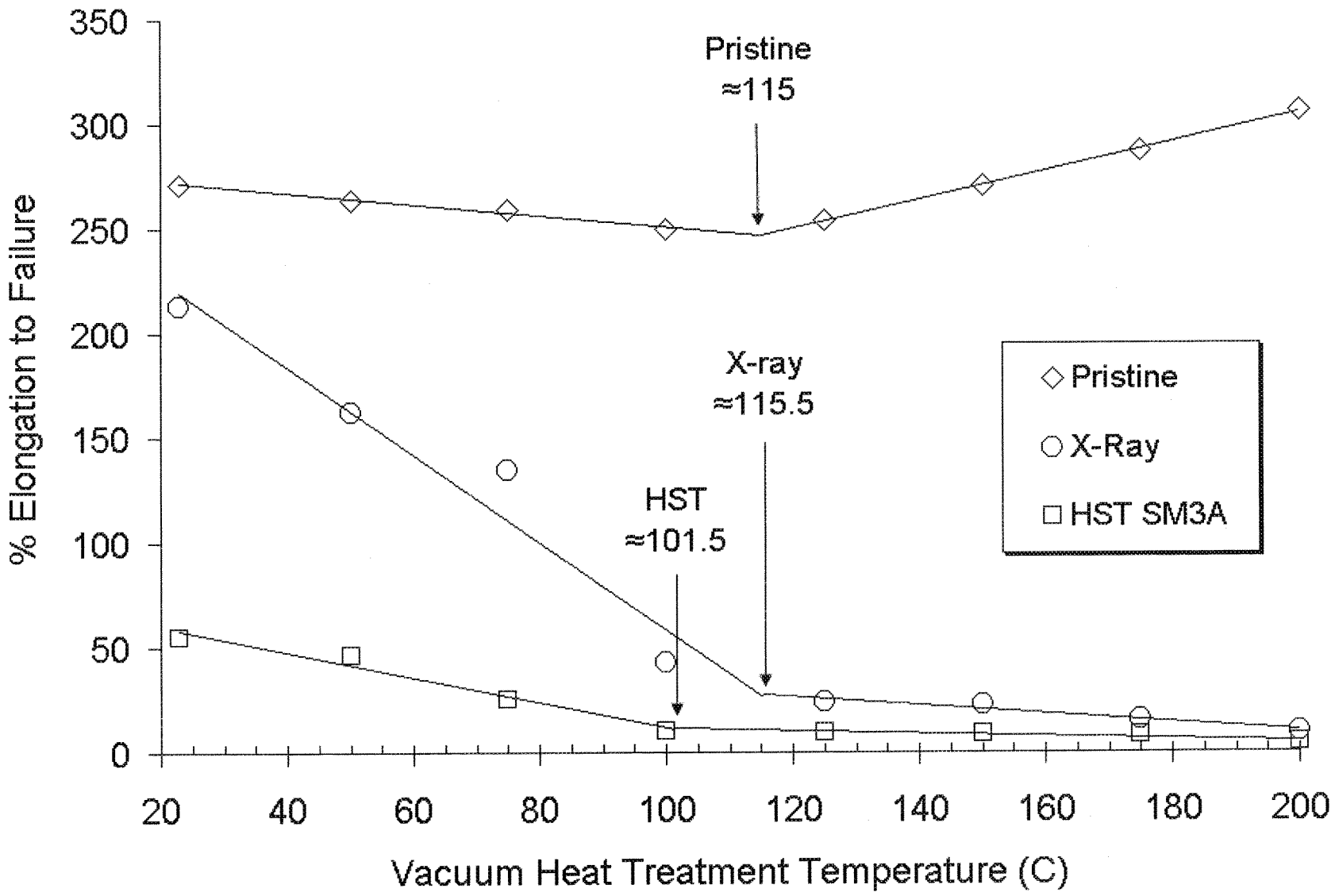
350
300
250
200
150
100
50
0
% Elongation to Failure
20
40
60
80
100
120
140
160
180
200
Vacuum Heat Treatment Temperature (C)
Pristine
≈115
X-ray
≈115.5
HST
≈101.5
Pristine
X-Ray
HST SM3A

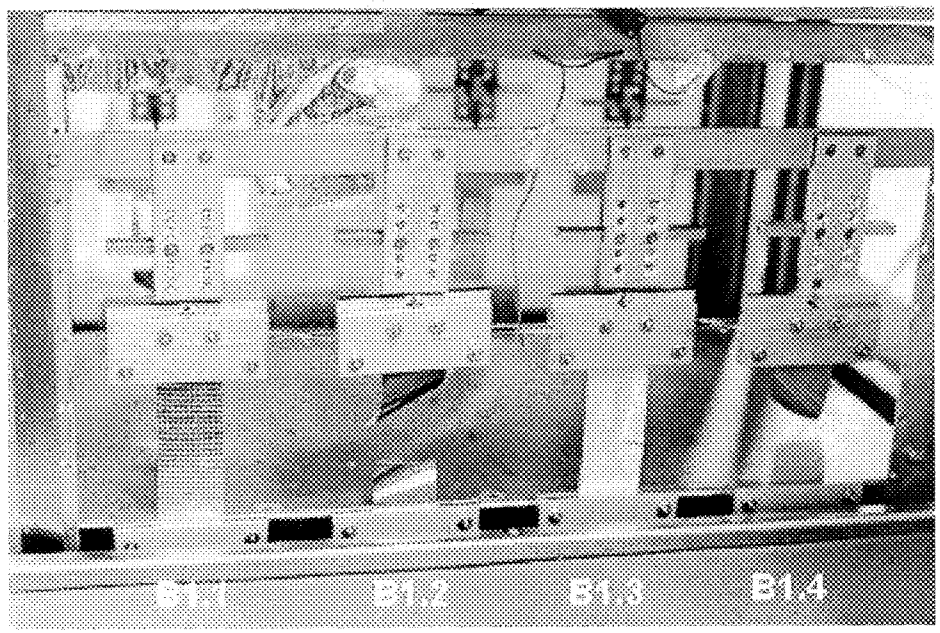

24 a

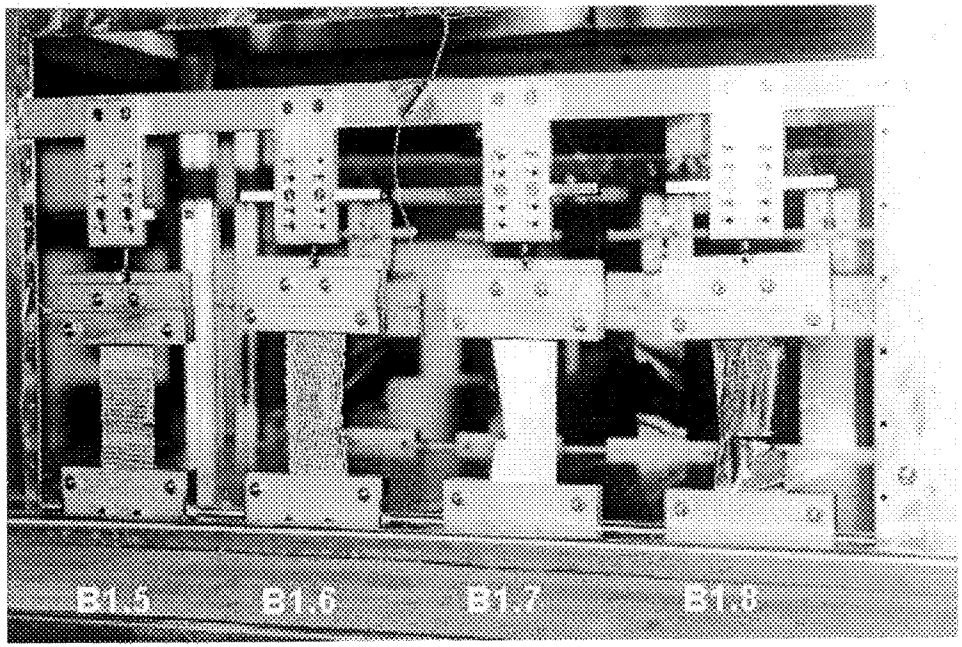

24 b

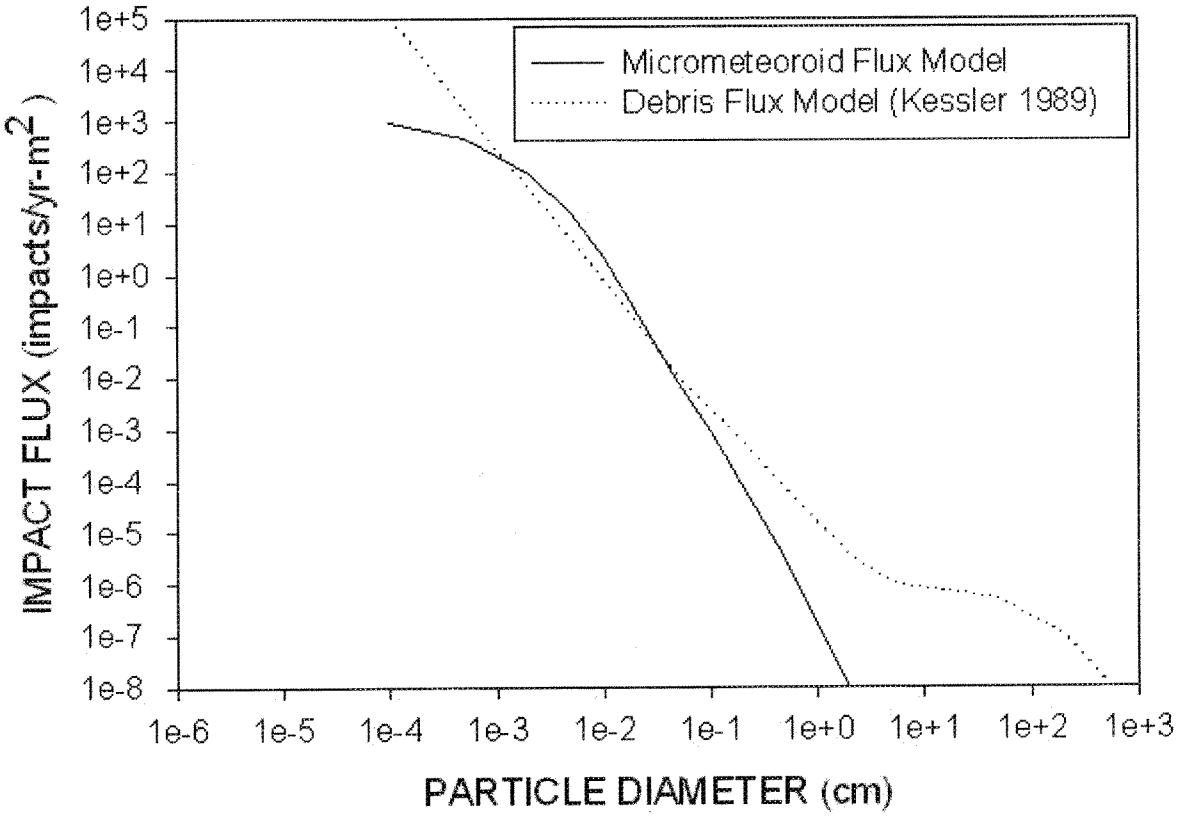
Micrometeoroid Flux Model
Debris Flux Model (Kessler 1989)
IMPACT FLUX (impacts/yr-m2)
1e+5
1e+4
1e+3
1e+2
1e+1
1e+0
1e-1
1e-2
1e-3
1e-4
1e-5
1e-6
1e-7
1e-8
1e-6
1e-5
1e-4
1e-3
1e-2
1e-1
1e+0
1e+1
1e+2
1e+3
PARTICLE DIAMETER (cm)

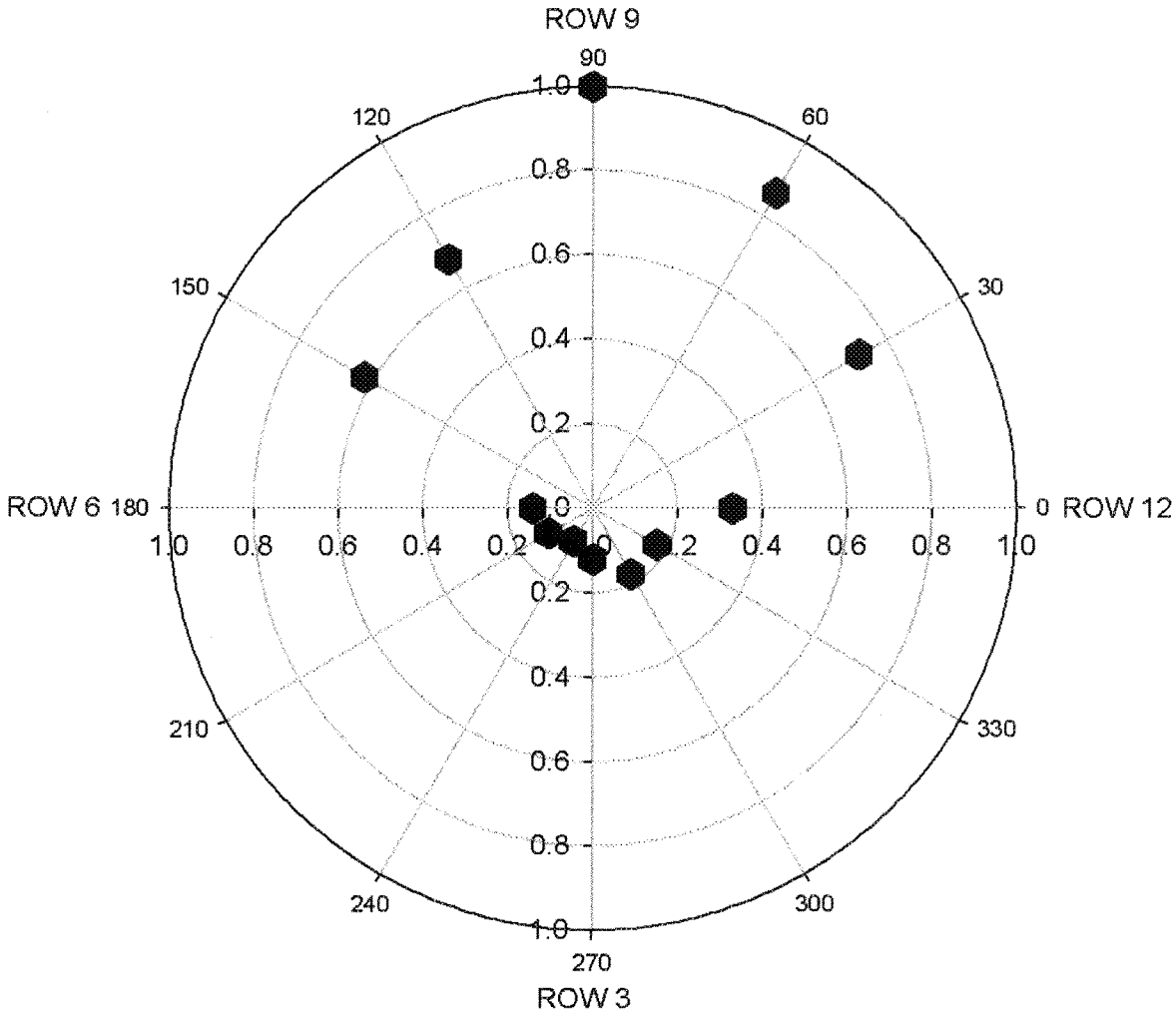
ROW 9
90
120
60
150
30
ROW 6
180
0
ROW 12
210
330
240
300
270
ROW 3
1.0
0.8
0.6
0.4
0.2
0

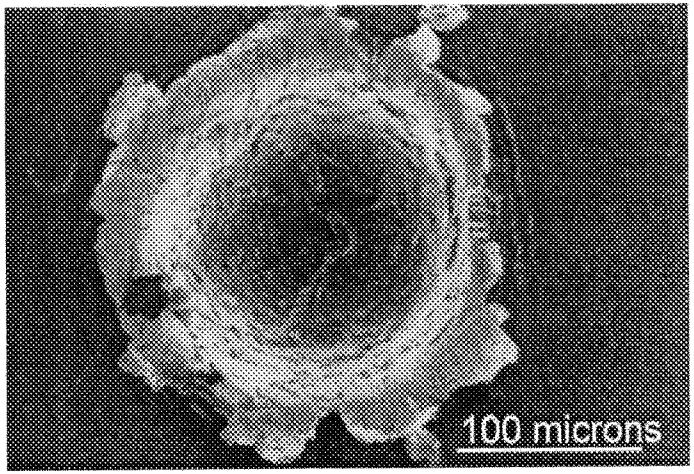

27 a

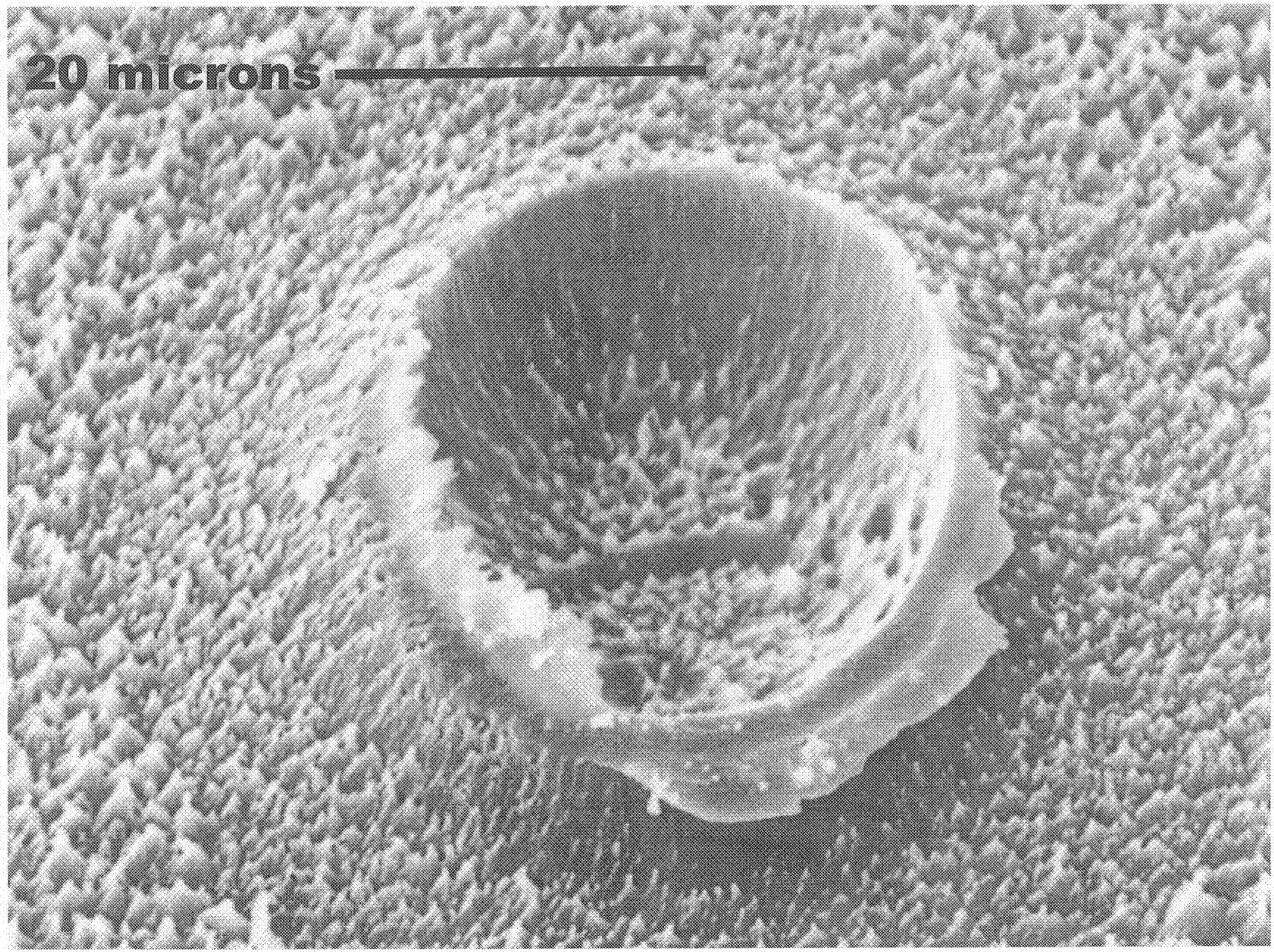

27 b

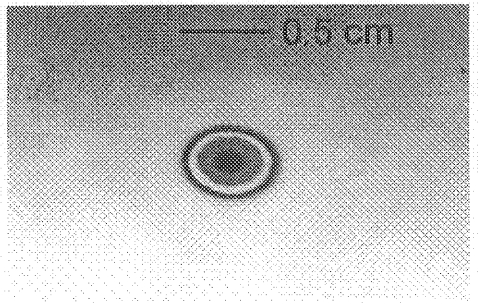
0.5 cm